Observations of radiocarbon in CO_2 at seven global sampling sites in the Scripps flask network: Analysis of spatial gradients and seasonal cycles

Heather D. Graven,[1,2] Thomas P. Guilderson,[3,4] and Ralph F. Keeling[1]

Received 11 July 2011; revised 9 November 2011; accepted 16 November 2011; published 25 January 2012.

[1] High precision measurements of $\Delta^{14}C$ were conducted for monthly samples of CO_2 from seven global stations over 2- to 16-year periods ending in 2007. Mean $\Delta^{14}C$ over 2005–07 in the Northern Hemisphere was 5 ‰ lower than $\Delta^{14}C$ in the Southern Hemisphere, similar to recent observations from I. Levin. This is a significant shift from 1988–89 when $\Delta^{14}C$ in the Northern Hemisphere was slightly higher than the South. The influence of fossil fuel CO_2 emission and transport was simulated for each of the observation sites by the TM3 atmospheric transport model and compared to other models that participated in the Transcom 3 Experiment. The simulated interhemispheric gradient caused by fossil fuel CO_2 emissions was nearly the same in both 1988–89 and 2005–07, due to compensating effects from rising emissions and decreasing sensitivity of $\Delta^{14}C$ to fossil fuel CO_2. The observed 5 ‰ shift must therefore have been caused by non-fossil influences, most likely due to changes in the air-sea ^{14}C flux in the Southern Ocean. Seasonal cycles with higher $\Delta^{14}C$ in summer or fall were evident at most stations, with largest amplitudes observed at Point Barrow (71°N) and La Jolla (32°N). Fossil fuel emissions do not account for the seasonal cycles of $\Delta^{14}C$ in either hemisphere, indicating strong contributions from non-fossil influences, most likely from stratosphere-troposphere exchange.

Citation: Graven, H. D., T. P. Guilderson, and R. F. Keeling (2012), Observations of radiocarbon in CO_2 at seven global sampling sites in the Scripps flask network: Analysis of spatial gradients and seasonal cycles, *J. Geophys. Res.*, *117*, D02303, doi:10.1029/2011JD016535.

1. Introduction

[2] Atmospheric sampling programs were initiated in the 1950s and 1960s to collect CO_2 at several locations for measurement of the ratio $^{14}C/C$ [*Rafter and Fergusson*, 1957; *Münnich*, 1963; *Nydal*, 1963]. Observations of $^{14}C/C$ ratios are typically reported as $\Delta^{14}C$, in part per thousand or ‰ deviations from the Modern Standard with a correction for mass-dependent fractionation using concurrent measurements of $^{13}C/^{12}C$ ratios [*Stuiver and Polach*, 1977]. The early observations of $\Delta^{14}C$ in CO_2 recorded a large increase between 1955 and 1964 caused by anthropogenic ^{14}C production from intensive nuclear weapons testing [*Nydal*, 1963; *Levin et al.*, 1985; *Manning et al.*, 1990]. The nuclear explosions carried most of the ^{14}C to high altitudes in the Northern Hemisphere where seasonal mixing of highly enriched air from the stratosphere into the troposphere caused seasonal variations of 100 ‰ at surface sites [*Lal and Rama*, 1966; *Randerson et al.*, 2002]. $\Delta^{14}C$ rose to nearly 1000 ‰ in the Northern Hemisphere but reached only 700 ‰ in the Southern Hemisphere, so that an interhemispheric gradient of 100 ‰ or more existed for several years [*Levin et al.*, 1985; *Manning et al.*, 1990; *Nydal and Lövseth*, 1996]. These observations of $\Delta^{14}C$ gradients and seasonal cycles provided insight on the rates and seasonality of across-tropopause and across-equator transport [*Lal and Rama*, 1966; *Nydal*, 1968; *Kjellström et al.*, 2000].

[3] Tropospheric $\Delta^{14}C$ levels peaked in the mid-1960s after the majority of testing ceased and the oceanic and terrestrial reservoirs continued to assimilate the excess ^{14}C. Observations of the intrusion of excess ^{14}C into the ocean by oceanic surveys conducted in the 1970s and 1990s have provided estimates of the rate of air-sea gas exchange and decadal scale water mass transport in the ocean interior [*Broecker et al.*, 1985; *Nydal*, 2000; *Sweeney et al.*, 2007]. The distinctive peak and subsequent decline in $\Delta^{14}C$ have also provided a marker for tracing the age of various types of terrestrial organic carbon [*Trumbore*, 2000]. Characterization of $\Delta^{14}C$ in CO_2 by atmospheric observations has been integral to these applications, and has additionally enabled

[1]Scripps Institution of Oceanography, University of California, San Diego, La Jolla, California, USA.
[2]Institute of Biogeochemistry and Pollutant Dynamics, ETH Zurich, Zurich, Switzerland.
[3]Center for Accelerator Mass Spectrometry, Lawrence Livermore National Laboratory, Livermore, California, USA.
[4]Department of Ocean Sciences, University of California, Santa Cruz, California, USA.

0148-0227/12/2011JD016535

the estimation of a bomb-derived ^{14}C budget in the global carbon reservoirs as an independent check on oceanic inventories [*Hesshaimer et al.*, 1994; *Naegler et al.*, 2006].

[4] ^{14}C in CO_2 has also been perturbed by human activities through the release of fossil-derived CO_2 which has become devoid of ^{14}C over millions of years due to its radioactive decay with a mean lifetime of about 8,000 years. Release of fossil fuel CO_2 reduces the $^{14}C/C$ ratio of atmospheric CO_2 by dilution [*Suess*, 1955]. Significant atmospheric ^{14}C dilution had already occurred by 1950 [*Suess*, 1955; *Tans et al.*, 1979] and dilution is now the most important process causing the decline in atmospheric $\Delta^{14}C$ [*Levin et al.*, 2010; *Graven et al.*, 2012].

[5] A principal interest in $\Delta^{14}C$ observations is in developing applications that identify fossil fuel-derived CO_2 in the atmosphere by quantifying $\Delta^{14}C$ dilution. This method has mainly been applied to estimate local and regional additions of fossil fuel-derived CO_2 by comparing $\Delta^{14}C$ in polluted air to $\Delta^{14}C$ in background air [e.g., *Levin et al.*, 1989; *Meijer et al.*, 1996; *Turnbull et al.*, 2006; *van der Laan et al.*, 2010]. Fossil fuel combustion also contributes to spatial and seasonal variation in $\Delta^{14}C$ in background air, due to the localization of emissions in populated areas of the Northern Hemisphere and seasonal variation in emission and atmospheric transport [*Randerson et al.*, 2002; *Levin et al.*, 2010]. If other influences were well-known, the effect of fossil fuel combustion on spatial and seasonal variation in $\Delta^{14}C$ in background air could be determined. This would effectively provide an observation-based estimate of the transport of fossil fuel CO_2, which varies strongly between different atmospheric transport models [*Gurney et al.*, 2003; *Stephens et al.*, 2007; *Peylin et al.*, 2011]. Isolating fossil from non-fossil influences on the temporal and spatial patterns in $\Delta^{14}C$ of background air may also enable an observation-based means of estimating CO_2 emissions over the entire globe that would be useful for validating inventories [*Levin et al.*, 2010], separate from applications focusing on the validation of national or continental-scale emissions inventories by measuring $\Delta^{14}C$ gradients across polluted, continental regions [*Pacala et al.*, 2010; *Rayner et al.*, 2010]. In addition to developing the fossil fuel tracer for background air, a better understanding of ^{14}C exchange processes is also of intrinsic value since the exchange rates and internal dynamics of ^{14}C in land and ocean reservoirs also govern anthropogenic CO_2 uptake and storage [*Levin and Hesshaimer*, 2000; *Randerson et al.*, 2002].

[6] Improving our knowledge of $\Delta^{14}C$ dynamics in background air requires precise observations and high-resolution modeling. Observations by *Levin et al.* [2010] show that in the recent 2002–07 period, $\Delta^{14}C$ has been lower in the Northern Hemisphere than the Southern Hemisphere. This represents a shift from near equality between the hemispheres in the 1980s [*Levin et al.*, 1992; *Meijer et al.*, 2006]. *Levin et al.* [2010] demonstrated that the recent Northern Hemisphere $\Delta^{14}C$ deficit is smaller but also increasing more rapidly than expected from fossil fuel burning alone. Another strong influence on the interhemispheric $\Delta^{14}C$ gradient is the air-sea ^{14}C flux in the Southern Ocean, which opposes the fossil fuel influence and is likely to have changed over the 1980s to 2000s. In an extrapolation of global oceanic survey measurements, *Levin et al.* [2010] estimated that reduced Southern Ocean ^{14}C uptake decreased the interhemispheric $\Delta^{14}C$ gradient by about 4 ‰ between 1987 and 2007, similar to the observed decrease. However, in their summed estimate of all contributions, including small contributions from the terrestrial biosphere and nuclear power industry that enrich Northern Hemisphere $\Delta^{14}C$, the total interhemispheric gradient estimated by *Levin et al.* [2010] for the 1980s to 2000s did not match the observations; neither did the total gradient estimated in another study for the 1980s only [*Randerson et al.*, 2002]. The models used by *Levin et al.* [2010] and *Randerson et al.* [2002] predicted a Northern Hemisphere deficit in $\Delta^{14}C$ that was too strong and began too early, compared to observations. The observed interhemispheric $\Delta^{14}C$ gradient is therefore not fully explained.

[7] Seasonal cycles of $\Delta^{14}C$ for 1995–2005 reported by *Levin et al.* [2010] are clearly defined in the Northern Hemisphere, with peak-to-trough amplitudes ranging from 3–7 ‰ and maximum $\Delta^{14}C$ in September-October. Seasonal amplitudes did not change appreciably between the 1990s and 2000s. At tropical and Southern Hemisphere sites, seasonal cycles are small and not well-resolved compared to the measurement uncertainty [*Levin et al.*, 2010]. The Northern Hemisphere cycles are thought to be caused by three processes operating in phase with one another. First is the emission and transport of fossil fuel emissions, which causes the largest build-up of fossil fuel-derived CO_2 near the surface in winter and spring [*Randerson et al.*, 2002; *Erickson et al.*, 2008; *Turnbull et al.*, 2009; *Levin et al.*, 2010]. Second is the transport of ^{14}C-enriched air from the stratosphere, which occurs primarily in the midlatitudes and brings the most stratospheric air to the surface in summer and fall [*Appenzeller et al.*, 1996]. Finally, the terrestrial biosphere is returning bomb-derived excess ^{14}C back to the atmosphere, slightly enriching $\Delta^{14}C$ in Northern summer and fall [*Turnbull et al.*, 2009; *Levin et al.*, 2010].

[8] Current observations of $\Delta^{14}C$ in CO_2 of background air are limited to a small number of sites [*Levin et al.*, 2010; *Currie et al.*, 2009; *Turnbull et al.*, 2007], with only I. Levin presently conducting long-term measurements throughout both hemispheres. Observations at an expanded number of sites are needed to confirm the changing gradients and the seasonal patterns reported by *Levin et al.* [2010], to characterize the meridional gradient with higher resolution, to quantify vertical gradients and differences in seasonality with altitude, and to identify interannual variability.

[9] In this paper, we present atmospheric measurements of $\Delta^{14}C$ in CO_2 samples collected by the Scripps CO_2 Program at the Scripps Institution of Oceanography (SIO) and analyzed at Lawrence Livermore National Laboratory (LLNL). We report observations of $\Delta^{14}C$ in CO_2 from 6 sites: Point Barrow, Alaska, USA; Mauna Loa and Cape Kumukahi, Hawaii, USA; Cape Matatula, Samoa, USA and Palmer Station and the South Pole, Antarctica. These measurements were conducted together with measurements of $\Delta^{14}C$ in CO_2 from La Jolla, California, USA that are presented in the accompanying paper [*Graven et al.*, 2012] and also discussed here.

[10] We focus on demonstrating the seasonal cycles and spatial gradients in $\Delta^{14}C$ of CO_2, how they have changed in recent decades, and the contribution made by fossil fuel emissions. We compare patterns in our measurements, which span 2- to 16-year periods ending in 2007, to those of

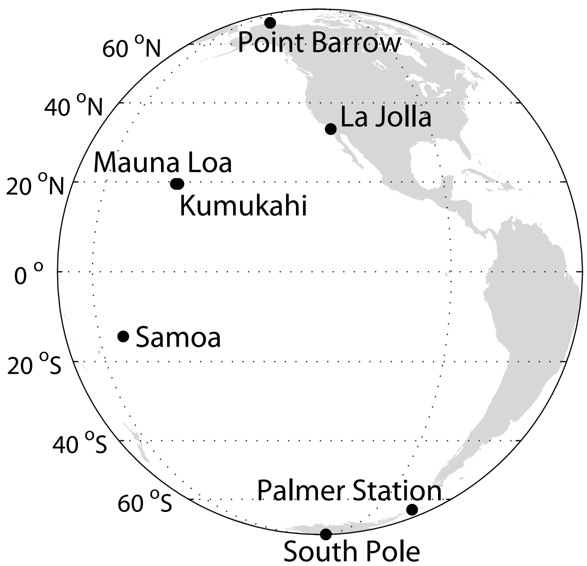

Figure 1. Clean air sampling stations in the SIO flask network where CO_2 samples were collected for $\Delta^{14}C$ analysis.

I. Levin [*Levin et al.*, 1992, 2010] at a different network of sites and to earlier measurements from the late 1980s and early 1990s at Point Barrow and the South Pole from *Meijer et al.* [2006]. We quantify the influence of fossil fuel emissions on spatial gradients and seasonal cycles in $\Delta^{14}C$ using transport model simulations of CO_2 emissions as specified by economic inventories, updating similar estimates by *Randerson et al.* [2002] and *Levin et al.* [2010] and applying these calculations specifically to the Scripps CO_2 observation sites. We thereby also quantify the spatial and seasonal variation in $\Delta^{14}C$ at these sites that is not associated with fossil fuel CO_2.

2. Methods

2.1. Observational Methods

[11] The sampling sites in the Scripps CO_2 Program where CO_2 samples have been collected for $\Delta^{14}C$ analysis are Point Barrow, Alaska (71.38°N, 156.47°W), La Jolla, California (32.87°N, 117.25°W), Mauna Loa, Hawaii (19.53°N, 155.58°W, 3397 m Above Mean Sea Level or AMSL), Kumukahi, Hawaii (19.52°N, 154.82°W), Cape Matatula, Samoa (14.25°S, 170.57°W), and the South Pole, Antarctica (89.98°S, 24.80°W, 2810 m AMSL); shown in Figure 1. Samples analyzed for $\Delta^{14}C$ were collected at roughly monthly intervals from La Jolla since 1992, from Point Barrow and the South Pole since 1999, with a year-long interruption from mid-2000 through mid-2001 at Point Barrow, and from Mauna Loa, Kumukahi and Samoa since 2001. At La Jolla, sampling occurs only under selected meteorological conditions with strong onshore winds, so that the sampled air is representative of the marine background composition despite the proximity of La Jolla to the highly populated Southern California region [*Graven et al.*, 2012]. Details on the sampling and analysis procedures of the Scripps CO_2 Program are provided in the accompanying paper [*Graven et al.*, 2012].

[12] Samples of CO_2 have also been collected for $\Delta^{14}C$ analysis from Palmer Station, Antarctica (64.92°S, 64.00°W; Figure 1) since 2005. Palmer Station is part of the sampling network of the Scripps O_2 Program which uses different flasks and sampling procedures than the Scripps CO_2 Program [*Keeling et al.*, 1998a]. The Scripps O_2 Program collects dry air in 5-liter spherical glass flasks with two stopcocks sealed by Viton® o-rings. To sample, air is freeze-dried and pumped through 3 flasks in series at 4 L min^{-1} for approximately 45 min. For flask air that is used for $\Delta^{14}C$ analysis, measurements of CO_2 concentration are performed using a Siemens infrared gas analyzer and measurements of $\delta(O_2/N_2)$ and $\delta(Ar/N_2)$ are performed using a MicroMass IsoPrime mass spectrometer at SIO. Remaining air undergoes cryogenic extraction to produce a pure CO_2 sample using the same methods as for the flasks from the Scripps CO_2 Program. Several tests were performed to confirm the comparability of $\Delta^{14}C$ in air sampled and analyzed in either flask type [*Graven*, 2008].

[13] All CO_2 samples were converted to graphite and analyzed at the Center for Accelerator Mass Spectrometry at LLNL between 2003 and 2009 [*Graven et al.*, 2007; *Graven*, 2008]. Details on $\Delta^{14}C$ analysis are provided in the accompanying paper [*Graven et al.*, 2012]. We report measurements in $\Delta^{14}C$ notation, utilizing the $\Delta^{14}C$ notation implicitly as a geochemical sample with known age and $\delta^{13}C$ correction [equivalent to Δ in the work by *Stuiver and Polach* [1977]). Uncertainty in $\Delta^{14}C$ for individual samples is ± 1.7 to ± 3.3 ‰, determined by the reproducibility of $\Delta^{14}C$ in CO_2 extracted from whole air reference cylinders [*Graven et al.*, 2007; *Graven*, 2008]. We present measurements for samples collected through the end of 2007. Due to limited sample supply, replicate samples were not available from stations other than La Jolla.

2.2. Atmospheric Transport Modeling of Fossil Fuel Emissions

[14] In order to quantify the effect of fossil fuel combustion on the observed $\Delta^{14}C$ gradients and seasonal cycles, we simulated the transport of fossil fuel-derived CO_2 in an atmospheric transport model. The dilution of $\Delta^{14}C$ by fossil fuel-derived CO_2 can be calculated by assuming the observed CO_2 concentration and $\Delta^{14}C$ is a mixture of fossil fuel-derived CO_2 and CO_2 from other sources including background air according to approximate mass balances for carbon and ^{14}C by:

$$\delta\Delta_{ff} = -\delta C_{ff} \frac{\Delta_M + 1000 \text{ ‰}}{C_M - \delta C_{ff}} \tag{1}$$

Here, $\delta\Delta_{ff}$ is the change in $\Delta^{14}C$ caused by fossil fuel-derived CO_2, δC_{ff} is the excess CO_2 concentration caused by the fossil fuel addition, and C_M and Δ_M are the observed CO_2 concentration and $\Delta^{14}C$. This equation is a rearrangement of the equation commonly used to calculate δC_{ff} using observations of $\Delta^{14}C$ in polluted air [e.g., *Meijer et al.*, 1996; *Levin et al.*, 2003; *Turnbull et al.*, 2006].

[15] We use this equation to estimate spatial gradients in $\delta\Delta_{ff}$ by defining δC_{ff} to be the difference in simulated C_{ff} between an observation site and the South Pole (Appendix A1). Choosing the South Pole as the reference site yields positive δC_{ff} at all other sites, but the interpretation would not change if any other site was arbitrarily chosen as the reference site. We use the same equation to estimate

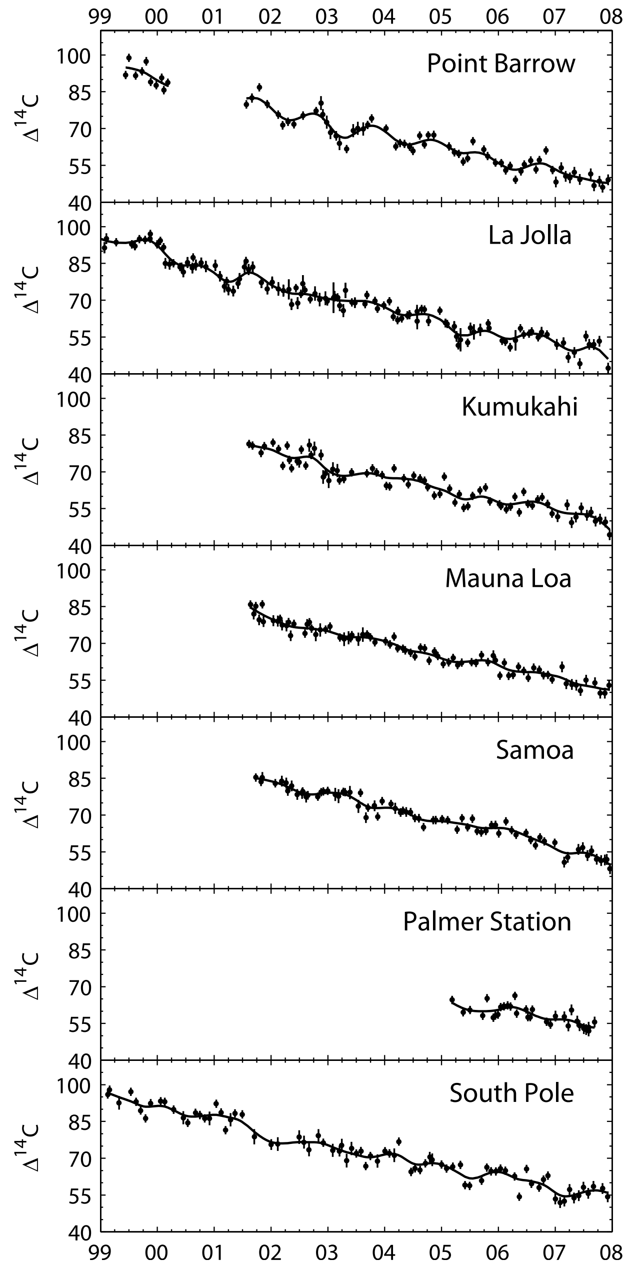

Figure 2. $\Delta^{14}C$ measured in CO_2 sampled at Point Barrow, La Jolla, Kumukahi, Mauna Loa, Samoa, Palmer Station and the South Pole. La Jolla measurements are repeated from Figure 1 of *Graven et al.* [2012] for the period 1999–2007. Error bars show measurement uncertainty of ±1.7 to ±3.3 ‰ in individual samples. Lines show cubic smoothing splines.

seasonal cycles of $\delta\Delta_{ff}$ by defining δC_{ff} to be the difference in simulated C_{ff} from the detrended annual mean value at each site (Appendix A2).

[16] We estimate δC_{ff} for individual years by performing 4-year forward simulations of the TM3 atmospheric transport model, following the procedure of the Transcom 3 Experiment to estimate steady state CO_2 gradients [*Gurney et al.*, 2000, 2003]. The TM3 model we use has 4° latitude by 5° longitude horizontal resolution with 19 vertical levels [*Heimann and Korner*, 2003] and a 6 hr time step, and uses National Center for Environmental Prediction (NCEP) reanalysis products [*Kalnay et al.*, 1996] specific to each year as meteorological forcing. Annual CO_2 source patterns of fossil fuel combustion and cement manufacturing were specified by the Emission Database for Global Atmospheric Research (EDGAR) version 4.0 (European Commission, 2009, http://edgar.jrc.ec.europa.eu/index.php; hereinafter European Commission, EDGAR, 2009), aggregated from 0.1 × 0.1° resolution to the 4 × 5° grid of the TM3 model. For the years 2006 and 2007, which were not included in the EDGAR database, we scaled the pattern of emissions for 2005 by 3% and 6% for 2006 and 2007, respectively, based on the estimated increase in global emissions [*Canadell et al.*, 2007; *Marland et al.*, 2008]. We use output from the 4th year of the 4-year forward simulations for individual years, interpolated at each observation site, except for the sites La Jolla, Point Barrow and Cape Grim, where we sampled the model at adjacent ocean grid cells according to the Transcom 3 Experimental Protocol [*Gurney et al.*, 2000]. To estimate transport uncertainty, we examine the range in δC_{ff} simulated by 16 atmospheric transport models [*Gurney et al.*, 2002, 2003]. Further details are given in Appendix A.

3. $\Delta^{14}C$ Observations

[17] Measurements of $\Delta^{14}C$ are shown at each station in Figure 2 together with cubic smoothing splines. We also compare $\Delta^{14}C$ observations from all stations by plotting the individual smoothing splines together in Figure 3. For La Jolla, the observations from 1999 through 2007 are repeated from Figure 1 of *Graven et al.* [2012]. $\Delta^{14}C$ measurements and uncertainties are listed in Appendix B; analogous data for La Jolla are listed in Appendix A of *Graven et al.* [2012]. These data are also available at the Scripps CO_2 Program Web site: http://scrippsco2.ucsd.edu/.

4. Trends in $\Delta^{14}C$, 2001–2007

[18] $\Delta^{14}C$ exhibited negative trends at all sites. For observations between mid-2001 and the end of 2007, the trends at Point Barrow, La Jolla, Kumukahi, Mauna Loa, Samoa and the South Pole were −5.0 ± 0.2, −5.0 ± 0.2, −4.7 ± 0.2, −4.8 ± 0.1, −5.2 ± 0.1 and −4.0 ± 0.2 ‰ yr^{-1}, respectively; trends and 1-σ uncertainties were quantified with linear least squares fits [*Cantrell*, 2008]. The South Pole appeared to have a trend that was roughly 20% smaller than the other stations over 2001–2007. The trend observed at Palmer Station between 2005 and 2007 was −3.8 ± 0.7 ‰ yr^{-1}, which is similar to the trend at the South Pole but not well resolved within the short observation period.

[19] Observed trends at all stations over 2001–07 were smaller than the trend of −5.5 ± 0.1 ‰ yr^{-1} observed at La Jolla over the longer period 1992–2007, consistent with a slowing in the rate of decrease of $\Delta^{14}C$ [*Graven et al.*, 2012]. Observations conducted at Point Barrow and the South Pole at the Groningen Laboratory (CIO) by *Meijer et al.* [2006] for 1985–91 showed linear trends of −10.3 ± 0.3 ‰ yr^{-1} and −10.4 ± 0.3 ‰ yr^{-1}. Comparing the trends at Point Barrow and the South Pole from *Meijer et al.* [2006] to our recent observations demonstrates reductions of 50–60% in the rate of decrease of $\Delta^{14}C$ between 1985–91 and 2001–07. As shown by *Graven et al.* [2012] and *Levin et al.* [2010], slowing of the rate of decrease in tropospheric $\Delta^{14}C$

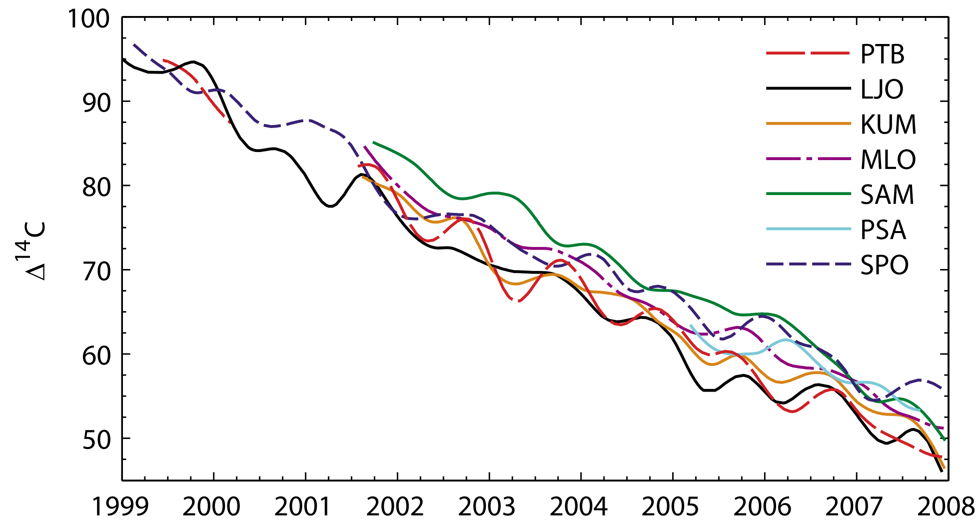

Figure 3. Cubic smoothing splines fitted to $\Delta^{14}C$ observations at each station. Sites in the Northern Hemisphere are represented by warmer colors. Spline curves were also shown individually in Figure 2.

over the 1980s–2000s was caused mainly by weakening oceanic ^{14}C uptake.

5. Meridional Gradients in $\Delta^{14}C$

5.1. Observed Gradients

[20] $\Delta^{14}C$ at Southern Hemisphere sites was generally higher than $\Delta^{14}C$ at Northern Hemisphere sites (Figure 3). CO_2 at La Jolla most commonly exhibited the lowest $\Delta^{14}C$ while CO_2 at Samoa most commonly exhibited the highest $\Delta^{14}C$. Interhemispheric gradients were largest from January through June, when $\Delta^{14}C$ in the Northern Hemisphere was at the seasonal minimum, thus reinforcing the annual mean gradient. The differences in $\Delta^{14}C$ between the stations varied interannually but did not show any long-term trends except possibly in relation to the South Pole, where $\Delta^{14}C$ appeared to increase relative to other sites after 2003. This characteristic is consistent with the fitted linear trend at the South Pole, which was less steep than the other stations over 2001–07 (Section 4), and with observations by *Levin et al.* [2010] that show $\Delta^{14}C$ increased at Neumayer, Antarctica, relative to other sites, in the early 2000s.

[21] Figure 4a shows the mean $\Delta^{14}C$ observed between July 2005 and June 2007 at each station, the time period with observations at all sites. The mean value from the South Pole was subtracted from all stations for plotting purposes. Means were computed for each station by fitting a linear trend and one annual harmonic to the observed $\Delta^{14}C$ between March 2005 and September 2007, then evaluating the fits over the period July 2005 through June 2007 and averaging. The error bars indicate the standard deviation of the residual difference between the observations and the fit at each station over the March 2005 through September 2007 period divided by the square root of the degrees of freedom in the fitted curves, given by the number of observations in that period minus the 4 fitted parameters. Uncertainty in mean values averaged ± 0.5 ‰.

[22] In 2005–07, Northern Hemisphere sea level sites were 5.1 ± 0.9 ‰ lower than the South Pole. Samoa showed the highest average $\Delta^{14}C$ relative to the South Pole ($+0.6 \pm 0.9$ ‰) and La Jolla showed the lowest (-5.9 ± 0.9 ‰). $\Delta^{14}C$ also tended to increase with increasing altitude, the South Pole was 1.8 ± 0.9 ‰ higher in $\Delta^{14}C$ than Palmer Station and Mauna Loa was 2.2 ± 0.7 ‰ higher than Kumukahi.

[23] Figure 4a also shows mean $\Delta^{14}C$ from January 1988 through December 1989 for the South Pole and Point Barrow [*Meijer et al.*, 2006] and for the stations Neumayer, Antarctica; Cape Grim, Australia; Izaña, Spain, and Jungfraujoch, Switzerland which are part of the observation network of Heidelberg University run by I. Levin [*Levin et al.*, 1990, 1992; *Levin and Kromer*, 2004]. Mean values for 1988–89 were computed using the same technique as for 2005–2007 over the period of September 1987 through March 1990. The uncertainty in mean $\Delta^{14}C$ for the 1988–89 observations averaged ± 0.8 ‰. By comparing observations from the Heidelberg and CIO laboratories, we assume that interlaboratory offsets are small, even though they have not yet been assessed by intercomparison activities [*Meijer et al.*, 2006]. Mean values for Izaña calculated with observations from the Trondheim laboratory [*Nydal and Lövseth*, 1996] were 0.9 ‰ lower than from *Levin et al.* [1992], which is similar to the uncertainty. The consistency in mean $\Delta^{14}C$ at Izaña suggests the laboratory offset between the Heidelberg and Trondheim laboratories is potentially less than ± 1 ‰.

[24] In 1988–89, $\Delta^{14}C$ was similar to the South Pole at all stations except Neumayer, on the Antarctic coast, where $\Delta^{14}C$ was 7.2 ± 1.3 ‰ lower than the South Pole. Observations from 1994, not shown, of $\Delta^{14}C$ gradients between sites in the Heidelberg network also showed little difference between the Northern and Southern Hemispheres though, interestingly, the strong gradient between Neumayer and Cape Grim observed in 1988–89 was absent in 1994 [*Levin and Hesshaimer*, 2000].

[25] By continuing the records at the sites in the Heidelberg network, *Levin et al.* [2010] found that Northern Hemisphere $\Delta^{14}C$ decreased relative to the Southern Hemisphere between the 1980s and 2000s, leading to a

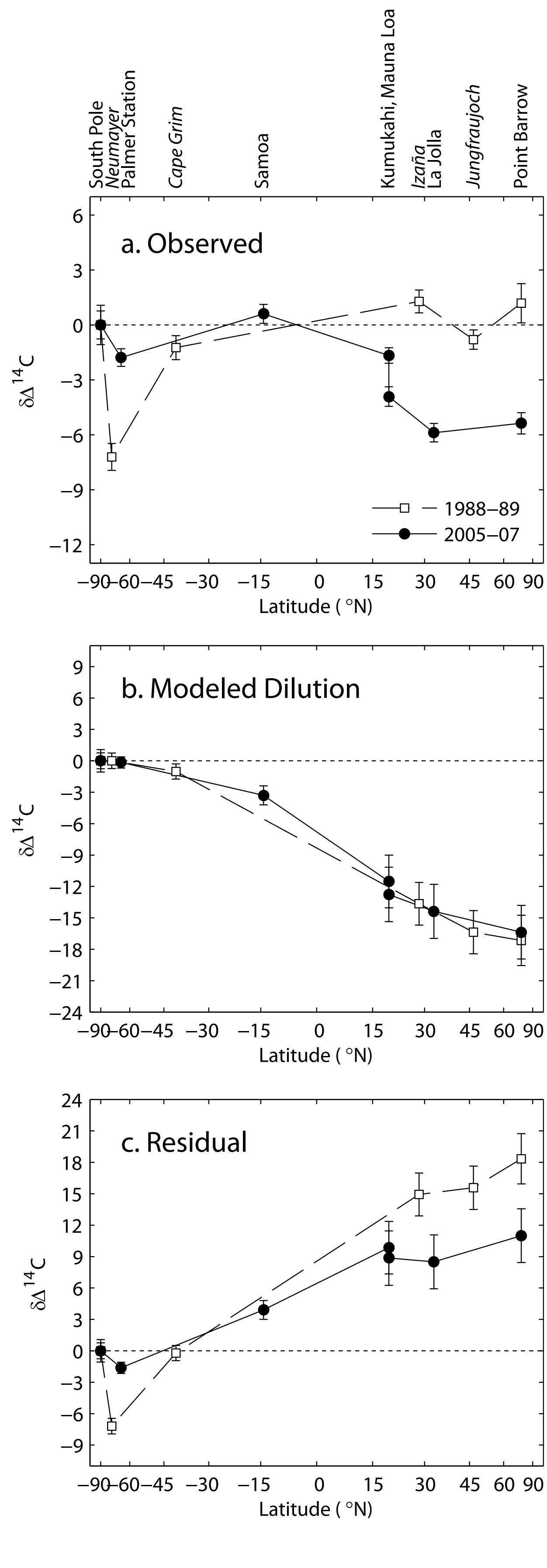

Northern deficit in $\Delta^{14}C$. Comparing our recent observations in the Scripps CO_2 network with the previous measurements also demonstrates a significant Northern deficit of about 5 ‰ developed (Figure 4a). Within the Scripps CO_2 network, a direct comparison can be made for the Point Barrow (71°N) - South Pole pair, which were both measured at CIO for the early period and at LLNL in the later period. The Point Barrow - South Pole gradient shifted from 1.2 ± 1.5 ‰ in 1988–89 to −5.4 ± 1.0 ‰ in 2005–07. A similar comparison is possible between 30°N and the South Pole using La Jolla (33°N) in 2005–07 and at Izaña (28°N) in 1988–89. The 30°N -South Pole difference decreased from 1.3 ± 1.2 ‰ to −5.9 ± 0.9 ‰. The consistency in trends at Point Barrow and 30°N relative to the South Pole indicate that a large-scale change occurred during this time frame.

[26] In contrast, the observed gradients between the South Pole and the coastal Antarctic sites (Neumayer or Palmer Station) cannot yet be interpreted to represent a systematic change in $\Delta^{14}C$ gradients over the high southern latitudes. *Levin et al.*'s [2010] record of the $\Delta^{14}C$ gradient between Neumayer and Cape Grim between 1987 and 2006 shows large interannual variations ranging from +1 to −7 ‰, suggesting the air sampled above the Southern Ocean is subject to strong variability and/or the observations at Neumayer may be subject to measurement artifacts.

5.2. Meridional Gradients in $\Delta^{14}C$ From Fossil Fuel Burning

[27] Our transport model simulations (Section 2.2 and Appendix A1) show that emissions of fossil fuel CO_2 strongly dilute $\Delta^{14}C$ in the Northern Hemisphere (Figure 4b), since nearly all fossil fuel emissions occur in the Northern Hemisphere (European Commission, EDGAR, 2009). Fossil fuel emissions reduced $\Delta^{14}C$ by an average of 15.8 ‰ at Northern sites, relative to the South Pole, in 1988–89. In 2005–07, fossil fuel emissions similarly reduced $\Delta^{14}C$ by an average of 14.9 ‰ at Northern sites (not including Mauna Loa).

[28] The fossil fuel dilution effect did not change significantly, despite the increase in emissions by roughly 50% from 1988–89 to 2005–07 [*Marland et al.*, 2008] (also European Commission, EDGAR, 2009). This can be

Figure 4. (a) Observed differences in mean $\Delta^{14}C$ (Δ_M) between each station and the South Pole for 1988 through 1989 (empty squares) and for mid-2005 through mid-2007 (black circles). Error bars indicate uncertainty in Δ_M at each station. Mean $\Delta^{14}C$ for 1988 through 1989 utilizes observations from *Levin et al.* [1990, 1991, 1992]; *Levin and Kromer* [2004] and *Meijer et al.* [2006]. Stations labeled in italics reflect sites in the Heidelberg network. (b) Dilution of $\Delta^{14}C$ by local fossil fuel CO_2 present at each site ($\delta\Delta_{ff}$), relative to the South Pole, as simulated by the TM3 4 × 5° atmospheric transport model using emissions from the EDGAR v4.0 database. (c) Residual $\Delta^{14}C$ (Δ_0) after subtracting fossil fuel dilution, presumably caused by regional carbon and ^{14}C exchanges with the ocean, biosphere and/or stratosphere and nuclear energy production. See Section 2.2 and Appendix A1 for a detailed description of the fossil fuel dilution and uncertainty estimations.

explained by changes in atmospheric composition concurrent with rising emissions [*Levin et al.*, 2010], which also determine the effect of adding fossil fuel CO_2 (equation (1)). Average atmospheric $\Delta^{14}C$ decreased from roughly 170 ‰ in 1988–89 to 60 ‰ in 2005–07, reducing the isotopic disequilibrium between CO_2 and fossil carbon, while CO_2 concentration rose from 350 ppm to 380 ppm, reducing the fractional change in CO_2 concentration per added increment of fossil-derived CO_2 (e.g. per Gt C emitted). Together, these changes reduced the sensitivity of atmospheric $\Delta^{14}C$ to fossil fuel emissions in 2005–07 compared to 1988–89. Additionally, growth in emissions in the northern subtropics and stagnant emissions in the northern midlatitudes between the 1980s and 2000s [*Andres et al.*, 2011] slightly reduced δC_{ff} simulated at high northern latitudes relative to subtropical latitudes in 2005–07.

[29] Our estimate of the fossil fuel component to the interhemispheric $\Delta^{14}C$ gradient using the TM3 model (−15 ‰) is similar to an estimate by *Turnbull et al.* [2009] for 2002–2007 (−16 ‰) from a different atmospheric transport model. By using higher resolution 3-D models, we and *Turnbull et al.* [2009] both improve upon *Levin et al.*'s [2010] estimate using a tropospheric 6-box model. *Turnbull et al.* [2009] and our estimates are also larger than *Levin et al.*'s [2010] estimate (−10 ‰), indicating the simulated gradients are sensitive to model resolution and model physics.

5.3. Meridional Gradients in $\Delta^{14}C$ From Other Processes

[30] The previous analysis shows that the observed shift to a Northern $\Delta^{14}C$ deficit between 1988–89 and 2005–07 is almost entirely due to processes other than fossil fuel burning. To quantify the non-fossil contribution to the gradient, we calculate the residual between the measured gradient and that predicted from fossil fuel burning, $\Delta_0 = \Delta_M - \delta\Delta_{ff}$ (Figure 4c). In both time periods, higher values of Δ_0 are found in the North compared to the South, with the difference decreasing from 16.4 ‰ in 1988–89 to 9.8 ‰ in 2005–07. The gradient in Δ_0 between Kumukahi and Mauna Loa is less than half of the observed gradient, indicating that fossil fuel CO_2 contributes to vertical gradients of $\Delta^{14}C$ in the Northern Hemisphere.

[31] *Levin et al.* [2010] estimated the contribution of air-sea exchange to the shifting gradient by extrapolating oceanic survey measurements conducted in the 1990s [*Key et al.*, 2004]. We expand on their estimate by comparing recent observations of $\Delta^{14}C$ in the surface of the Southern Ocean from *Jenkins et al.* [2010] to the prior measurements from *Key et al.* [2004]. In 2005, the air-sea gradient averaged 80 ‰ across the latitudes 44–63°S in the Pacific sector of the Southern Ocean, while in 1991 the air-sea gradient averaged 130 ‰. The fractional decrease in the air-sea gradient (40%) is similar to the fractional decrease in Δ_0 (Figure 4c), indicating that reduced ^{14}C uptake to the Southern Ocean is likely to be the main driver of the shifting gradient. This estimate is consistent with Levin's extrapolation, which resulted in a decrease in the interhemispheric $\Delta^{14}C$ gradient of about 4 ‰ between 1987 and 2007, which was similar to the observed decrease. It is also consistent in sign with a reduced influence of air-sea exchange on global tropospheric $\Delta^{14}C$ in the 2000s, compared to the 1990s, as simulated with an oceanic box diffusion model in the accompanying paper [*Graven et al.*, 2012].

[32] Other contributions to meridional gradients of $\Delta^{14}C$ are unlikely to have changed as much as the air-sea exchange in the Southern Ocean. Emissions of ^{14}C by the nuclear industry cause a small Northern $\Delta^{14}C$ excess since they occur almost entirely in the Northern Hemisphere. But this contribution is small and is likely to have increased slightly in recent decades, in opposition to the observed change [*Levin et al.*, 2010; *Graven and Gruber*, 2011]. Similarly, exchanges with ^{14}C-enriched terrestrial ecosystems induce a small Northern $\Delta^{14}C$ excess that is likely to have increased slightly in recent decades, also in opposition to the observed change [*Levin et al.*, 2010].

6. Seasonal Cycles

[33] Figure 5 shows the mean seasonal cycles in $\Delta^{14}C$ for mid-2001 to 2007. Average cycles were computed by first subtracting the fitted linear trend for each station (Section 4), except Palmer Station, then binning by month and averaging. For Palmer Station, observations were detrended using the average of the fitted trends at Samoa and the South Pole, −4.6 ‰ yr^{-1}.

[34] The seasonal cycles generally show a pattern with minima in $\Delta^{14}C$ occurring in spring and maxima in the late summer or fall. The average seasonal peak-to-trough amplitude appeared to decrease progressing southward in the Northern Hemisphere from Point Barrow (71°N, ∼7 ‰) to La Jolla (33°N, ∼5 ‰) to Kumukahi (20°N, ∼4 ‰). Low seasonal peak-to-trough amplitude of 2–3 ‰ was observed at Mauna Loa and Samoa. At the South Pole, monthly values that were consistently different than average were only apparent for the spring months when ^{14}C was enriched.

[35] Seasonal cycles at Point Barrow and the South Pole from the earlier period 1985–1991 [*Meijer et al.*, 2006] were computed in the same manner and are also shown in Figure 5. The cycles are generally similar between periods. The amplitude at Point Barrow appeared to decrease by roughly 30%, although with large uncertainty. Seasonal variation at the South Pole in both periods showed highly variable $\Delta^{14}C$ that tended to be enriched at the end of the calendar year. A strong maximum in December averaging 5 ‰ in the 1985–91 observations was larger than the average enrichment of 1–3 ‰ over spring months in 2001–07.

[36] Figure 5 also shows the simulated cycles in $\Delta^{14}C$ from fossil fuel burning ($\delta\Delta_{ff,seas}$). The cycles were computed using 2 sets of TM3 simulations (Section 2.2 and Appendix A2) with either seasonally varying or aseasonal emissions. The seasonally varying emissions were implemented with a latitude-dependent sinusoidal amplitude factor of 30% [*Gurney et al.*, 2005], which produces amplitudes of ±15–25% in the midlatitudes with stronger emissions in January in the Northern Hemisphere and in July in the Southern Hemisphere. This likely overestimates the actual variation, since the sinusoidal function does not account for energy use for air conditioning during the summer months [*Blasing et al.*, 2004; *Gurney et al.*, 2005; *Erickson et al.*, 2008] and since the amplitude is toward the higher end of economic- and observation-based estimates [*Rotty*, 1987; *Levin et al.*, 2003; *Blasing et al.*, 2004]. We also show the range of $\delta\Delta_{ff,seas}$ simulated in the 16 Transcom models using

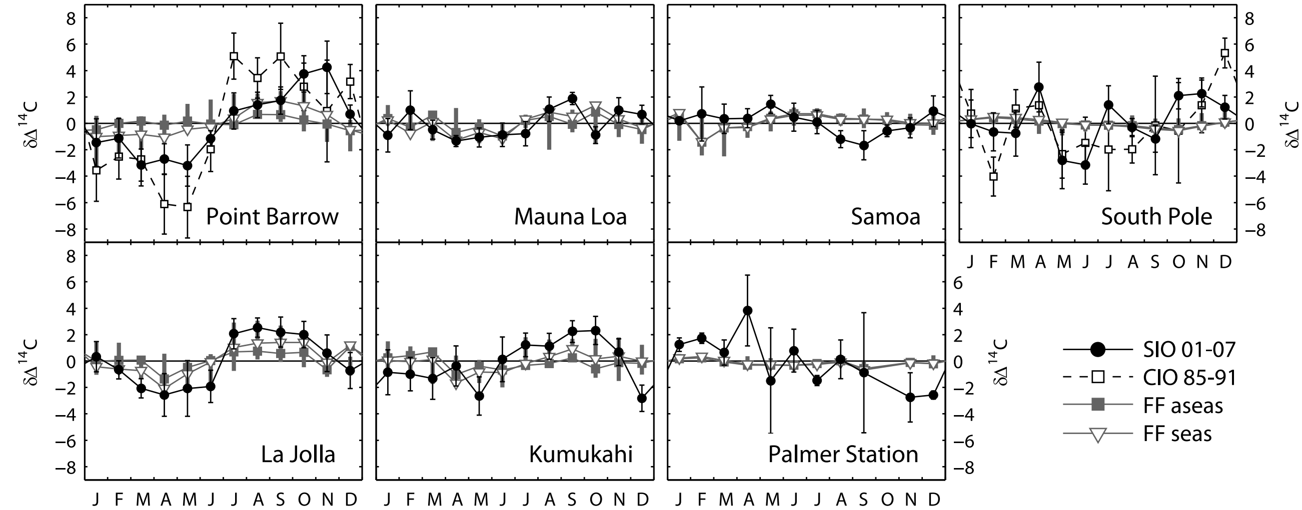

Figure 5. Mean and standard error of detrended $\Delta^{14}C$ in monthly bins for observations between mid-2001 and the end of 2007 (black circles and solid lines). For Point Barrow and the South Pole, the detrended mean and standard error is also shown for 1985–91 observations from CIO (empty squares and dashed lines [*Meijer et al.*, 2006]). Simulated fossil fuel CO_2 contributions to the seasonal cycles of $\Delta^{14}C$ are shown in gray, as calculated by equation (1) using output from the TM3 4 × 5° atmospheric transport model with annual emissions from the EDGAR v4.0 database that was sampled at the same times as the observations. Emissions were aseasonal (squares) or varied with a 30% seasonal amplitude factor (triangles). Also shown as thick gray vertical lines are the range of fossil fuel CO_2 contributions for 1995 simulated by 16 atmospheric transport models with aseasonal emissions in the Transcom 3 Experiment [*Gurney et al.*, 2003].

aseasonal emissions for 1995 as gray bars in Figure 5 (Appendix A2).

[37] Distinct seasonal cycles of $\delta\Delta_{ff,seas}$ were simulated at Point Barrow, La Jolla and Kumukahi (Figure 5). The modeled $\delta\Delta_{ff,seas}$ has similar phasing to the observations; however, the amplitude is considerably smaller than the observed cycles. This is true regardless of which transport model or whether aseasonal or seasonal emissions were used. At Samoa, a distinct seasonal cycle was also simulated for $\delta\Delta_{ff,seas}$; however, the phasing in $\delta\Delta_{ff,seas}$ is opposite to the observed phasing.

[38] The scatter in monthly averages shown in Figure 5 arises partly from measurement uncertainty in $\Delta^{14}C$, but also from interannual variability in the seasonal cycle, which can be seen in Figures 2 and 3. This interannual variability was not consistent over wide regions; for example, high amplitude was observed at Point Barrow in 2002 and 2003 while La Jolla showed low amplitude.

[39] In Figure 6, we investigate year-to-year variation in the seasonal amplitude and phase at La Jolla over 1992–2007. $\Delta^{14}C$ was detrended by subtracting a cubic smoothing spline with cutoff period of 24 months [*Graven et al.*, 2012], then each year was fit to a single harmonic to determine the peak-to-trough amplitude (Figure 6a) and the timing of maximum $\Delta^{14}C$ (Figure 6b) in each calendar year. We repeated the process for years defined as July to June to evaluate robustness in amplitude variations. Amplitude and phase in simulated $\delta\Delta_{ff,seas}$ were also calculated for each calendar year.

[40] The seasonal amplitude of $\Delta^{14}C$ observed at La Jolla varied between 1 and 8 ‰, but showed no apparent trend. The strong variations in seasonal cycles at La Jolla appear to be larger than at Jungfraujoch [*Levin et al.*, 2010], but strong variations in seasonal cycles have been observed at Wellington, New Zealand [*Currie et al.*, 2009]. Average amplitudes at Jungfraujoch (1986–2006) and Niwot Ridge, Colorado, USA (2003–05) were within the range of amplitude observed at La Jolla [*Levin and Kromer*, 2004; *Levin et al.*, 2010; *Turnbull et al.*, 2007], while the average amplitude at Point Barrow (2001–07) was higher (Figure 6). The simulated year-to-year variation in the amplitude of $\delta\Delta_{ff,seas}$ was small and not consistent with the observed variation.

[41] The maximum $\Delta^{14}C$ at La Jolla consistently occurred between August and November, except in 1993, 1995 and 2002–03 when the phase was poorly resolved due to low amplitude. The timing of maximum $\Delta^{14}C$ at La Jolla was similar to Point Barrow but one month later than Jungfraujoch and Niwot Ridge, on average. Observations from Vermunt, Austria (1959–84 [*Levin and Kromer*, 2004]) and Fruholmen, Norway (1963–93 [*Nydal and Lövseth*, 1996]) during and subsequent to the period of nuclear weapons testing showed maximum $\Delta^{14}C$ 1–2 months earlier than more recent observations at Jungfraujoch and Point Barrow, located at the same latitudes (47°N and 71°N, respectively).

7. Discussion

7.1. Meridional Gradients

[42] The shift in the meridional $\Delta^{14}C$ gradient from 1988–89 to 2005–07 appears to be consistent with weakened air-sea uptake in the Southern Ocean (Section 5.3 and

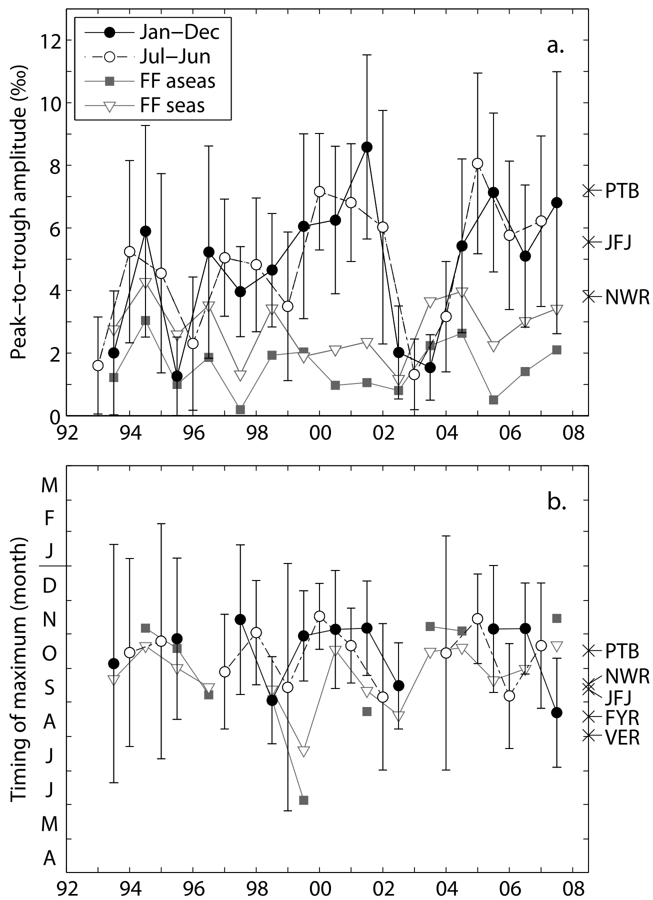

Figure 6. Results of fitting detrended $\Delta^{14}C$ at La Jolla to a single annual harmonic. (a) Peak-to-trough amplitude and (b) timing of maximum annual $\Delta^{14}C$. Calendar years defined as January to December are shown as the filled black circles and solid line; years defined as July to June are shown in the empty circles and dash-dotted line. Error bars reflect 1-σ uncertainties in the fitted harmonics. Also shown is the modeled amplitude and phase resulting from combustion and transport of fossil fuel ($\delta\Delta_{ff,seas}$), using aseasonal emissions (filled gray squares) or a 30% seasonal amplitude factor in emissions (empty gray triangles) from the EDGAR v4.0 database in the TM3 4 × 5° atmospheric transport model. Omitted years in Figure 6b had uncertainties larger than ±4 months. The crosses on the right axes show the average amplitude and/or timing of seasonal maximum $\Delta^{14}C$ at other Northern Hemisphere observation sites: Fruholmen, Norway (FYR, 71°N, 1963–1993 [*Nydal and Lövseth*, 1996]), Vermunt, Austria (VER, 47°N, 1959–1984), Jungfraujoch, Switzerland (JFJ, 47°N, 1986–2007 [*Levin and Kromer*, 2004]), Niwot Ridge, USA (NWR, 40°N, 2003–2005 [*Turnbull et al.*, 2007]) and Point Barrow (PTB, 2001–07).

Levin et al. [2010]); however, a comprehensive understanding of all individual contributions to the meridional $\Delta^{14}C$ gradient has not yet been achieved. Here, we only quantified the fossil fuel component. Other studies that have simulated all known contributions to $\Delta^{14}C$ gradients have not succeeded in matching the observed gradient [*Levin et al.*, 2010; *Randerson et al.*, 2002]. The sum of all components from *Levin et al.*'s [2010] study resulted in a simulated North - South gradient that was 3 ‰ lower than observed, and they could not match the observed gradient and long-term trend over 1987–2007 simultaneously by adjusting model parameters. *Randerson et al.* [2002] also simulated a total gradient that was 3 ‰ too low in the 1980s. Reconciliation of the observed $\Delta^{14}C$ gradient and trend will likely require improvements in the representation of ocean circulation and the age structure of respired carbon in global models.

[43] In the future, the meridional $\Delta^{14}C$ gradient can be expected to continue to shift in the same direction as rising fossil fuel CO_2 emissions decrease atmospheric $\Delta^{14}C$ further, weakening air-sea ^{14}C exchange in the Southern Ocean even more. At the same time, ^{14}C will continue to be released from the terrestrial biosphere and rapidly overturning ocean regions outside of the Southern Ocean. Precise observation of meridional $\Delta^{14}C$ gradients in the coming years and further investigation of historical gradients could provide insights on the carbon turnover in ocean and land reservoirs that govern regional $\Delta^{14}C$ disequilibria and ^{14}C fluxes.

7.2. Seasonal Cycles

[44] Fossil fuel CO_2 emission and transport contribute to seasonal cycles of $\Delta^{14}C$ at Northern Hemisphere sites; however, the observed seasonal cycles cannot be explained solely by fossil fuel influences. Model simulations of other known contributions to $\Delta^{14}C$ that were conducted by *Randerson et al.* [2002] and *Levin et al.* [2010] demonstrate a substantial seasonal influence from the stratosphere in mid- to high latitudes of both hemispheres, in addition to smaller contributions from the terrestrial biosphere in the North and air-sea exchange in the South. *Randerson et al.*'s [2002] simulated seasonal cycle for Fruholmen, Norway over 1985–90 is similar to the observations at Point Barrow for 1985–1991 from *Meijer et al.* [2006], which showed the same phasing but larger amplitude than our recent measurements at Point Barrow for 2005–07. The cause of the reduction in amplitude at Point Barrow is not presently known, and such a reduction in amplitude was not apparent at La Jolla or Jungfraujoch [*Levin et al.*, 2010] over the same period. Simulated seasonal cycles for northern and southern midlatitudes from *Levin et al.* [2010] were similar to observed cycles at La Jolla and Palmer Station.

[45] Contributions to the seasonal cycle should be expected to vary between midlatitude sites that reside at different altitudes. In particular, the influence of stratosphere-troposphere transport should contribute to larger and earlier seasonal maxima at higher altitude sites than sea level sites in the midlatitudes since closer proximity to the stratosphere would reduce the transport time and the attenuation in amplitude [*Liang et al.*, 2009]. Correspondingly, the $\Delta^{14}C$ maximum at high altitude sites Jungfraujoch and Niwot Ridge was observed one month earlier than at La Jolla and Point Barrow (Figure 6b). A one month delay was also observed in recent measurements at Alert (82°N) compared to Jungfraujoch [*Levin et al.*, 2010]. Average seasonal amplitudes, however, were not larger at Jungfraujoch and Niwot Ridge, compared to La Jolla or Point Barrow

(Figure 6a). One explanation for the lack of reduced amplitude at the sea level sites may be that an attenuated stratospheric influence is compensated by a larger influence from fossil fuel CO_2, which can be seen by comparing $\delta\Delta_{ff,seas}$ between Kumukahi and Mauna Loa. Another explanation may be that the $^{14}CO_2$ concentration in air of stratospheric origin increases with time after cross-tropopause transport, since some oxidation of cosmogenic radiocarbon from ^{14}CO occurs after entering the troposphere [*Jöckel et al.*, 2002]. The oxidation of ^{14}CO may also contribute to summertime enrichment in $\Delta^{14}C$ of CO_2, since oxidization occurs more rapidly in the summer. Seasonal peak-to-trough amplitudes of 10–15 molecules ^{14}CO cm^{-3} STP observed at Northern and Southern midlatitudes [*Jöckel and Brenninkmeijer*, 2002; *Manning et al.*, 2005] suggest that ^{14}CO oxidation in the lower troposphere may add approximately 1 ‰ amplitude to the seasonal cycle.

[46] Stratosphere-troposphere exchange may account for most of the variability in the seasonal amplitude of $\Delta^{14}C$ at mid- to high latitudes. The atmospheric eddies and tropopause folds that drive cross-tropopause transport have an episodic nature that causes the location and magnitude of stratosphere-troposphere exchange to vary significantly between years [*Gettelman and Sobel*, 2000; *James et al.*, 2003; *Stohl et al.*, 2003]. Modeling studies that resolve interannual variation in tropospheric ozone or Lagrangian particle transport caused by variable stratosphere-troposphere transport support this idea [e.g., *Sprenger and Wernli*, 2003; *James et al.*, 2003; *Cristofanelli et al.*, 2006], but simulations of the effect on seasonal cycles of long-lived trace gases have not yet been performed.

8. Summary

[47] Here and in the accompanying paper [*Graven et al.*, 2012] we report measurements of $\Delta^{14}C$ in CO_2 at seven global stations made through collaboration between the Scripps Institution of Oceanography flask sampling networks and Lawrence Livermore National Laboratory.

[48] Comparison of our measurements from 2005–07 with prior measurements from 1988–89 [*Levin et al.*, 1992; *Meijer et al.*, 2006] show that Northern Hemisphere $\Delta^{14}C$ has decreased by 5 ‰, relative to the Southern Hemisphere. Our observations are consistent with *Levin et al.* [2010], who observed a similar shift in the interhemispheric $\Delta^{14}C$ gradient. The simulated contribution to $\Delta^{14}C$ gradients from fossil fuel CO_2 emissions were nearly the same in 1988–89 and 2005–07, also in agreement with *Levin et al.* [2010]. These analyses demonstrate that the shift in the meridional $\Delta^{14}C$ gradient was not caused by increased fossil fuel combustion. The shift is likely to have been caused by decreasing ^{14}C uptake in the Southern Ocean, since the air-sea $\Delta^{14}C$ disequilibrium was reduced by a similar amount as the fossil fuel-corrected $\Delta^{14}C$ gradient between the 1990s and 2000s [*Levin et al.*, 2010; *Jenkins et al.*, 2010; *Key et al.*, 2004].

[49] Seasonal cycles with higher $\Delta^{14}C$ in summer and/or fall were observed at most stations. In the Northern Hemisphere, seasonal cycles were similar in phase to observations at other sites [*Levin et al.*, 2010; *Turnbull et al.*, 2007] and were partly explained by the seasonal emission and transport of fossil fuel-derived CO_2 as simulated by the TM3 model. Though not quantitatively modeled here, *Randerson et al.* [2002] and *Levin et al.* [2010] showed that stratosphere-troposphere transport provides a strong influence on seasonal cycles of $\Delta^{14}C$ in the Northern midlatitudes, while stratosphere-troposphere transport and air-sea exchange both influence seasonal cycles in the Southern Hemisphere. Our observations demonstrate substantial variability in the seasonal amplitude of $\Delta^{14}C$, particularly at La Jolla. This suggests that the specification of background $\Delta^{14}C$ levels, which is necessary for identifying additions of fossil fuel-derived CO_2 in polluted air, requires regular, precise measurements of $\Delta^{14}C$ at clean air sites.

Appendix A: Methods for Calculating Fossil Fuel Influences

A1. Meridional Gradients

[50] Simulated CO_2 concentrations resulting from fossil fuel emissions in the TM3 model (Section 2.2) for 1988 and 1989 were averaged to estimate δC_{ff} for 1988–89, and results from simulations for 2005, 2006 and 2007 were averaged with twice as much weight on 2006 to estimate δC_{ff} for mid-2005 to mid-2007. In each case, δC_{ff} was calculated by subtracting C_{ff} simulated for the South Pole. C_M in equation (1) was calculated by the average of monthly CO_2 observations from the Scripps CO_2 and O_2 Programs [*Keeling et al.*, 1998b, 2005], from the Instituto Nacional de Meteorologia for Izaña (http://gaw.kishou.go.jp/wdcgg/), and from the National Oceanic and Atmospheric Administration (NOAA) for Cape Grim [*Conway and Tans*, 2004]. No CO_2 observations were available at Neumayer and Jungfraujoch so their CO_2 concentrations were approximated using observations from Palmer Station and from Terceira Island, Azores conducted by NOAA [*Conway and Tans*, 2004].

[51] Uncertainties in $\delta\Delta_{ff}$ were estimated as a quadrature sum of four sources of uncertainty: the measurement uncertainty in Δ_M (Section 3.5 and Figure 4) and C_M, and the uncertainty in δC_{ff} caused by the uncertainty in fossil fuel CO_2 emissions and the uncertainty in transport of fossil-derived CO_2, both of which grow with increased emissions. Measurement uncertainty in C_M is ± 0.1 ppm [*Keeling et al.*, 1998b; *Conway and Tans*, 2004; *Keeling et al.*, 2005], except at Jungfraujoch and Neumayer where we increased the uncertainty in C_M to ± 0.4 ppm since observations were not available at these sites. We assigned the uncertainty in emissions as $\pm 10\%$, slightly larger than uncertainties in global emissions of $\pm 8\%$ estimated by *Andres et al.* [1996] and $\pm 5\%$ estimated by *Canadell et al.* [2007]. To estimate transport uncertainty, we used the standard deviation in annual mean δC_{ff} at each station simulated by the 16 atmospheric transport models that participated in the Transcom 3 experiment [*Gurney et al.*, 2002, 2003], using Plateau Rosa Station, Italy and the Pacific Ocean Station at 35°N, 143°W to represent Jungfraujoch and La Jolla. We scaled the standard deviation in the Transcom simulations for 1990 to the mean global emissions in 1988–89 and the standard deviation in the Transcom simulations for 1995 to the mean global emissions in 2005–07. The resulting uncertainty in transport was ± 0.6–2.8% at the Southern Hemisphere sites and ± 7.6–9.5% at the Northern Hemisphere sites. We note that

transport uncertainty may be even larger than the standard deviation between different models, due to biases in common model formulations or meteorological products. The largest contribution to uncertainty was the uncertainty in transport at Northern Hemisphere sites and uncertainty in Δ_M at Southern Hemisphere sites. Combining all four contributions, the total uncertainty in $\delta\Delta_{ff}$ averaged ±1.5 ‰ in 1988–89 and ±1.8 ‰ in 2005–07.

A2. Seasonal Cycles

[52] For each calendar year at each site, simulated CO_2 concentrations resulting from fossil fuel emissions in the TM3 model were detrended, sampled at the time steps nearest to the sampling times of the observations and used to calculate $\Delta^{14}C$ variations according to equation (1). Here, $\delta\Delta_{ff}$ is interpreted as the change in $\Delta^{14}C$ due to seasonal variation in fossil fuel CO_2 (noted by $\delta\Delta_{ff,seas}$). δC_{ff} is the modeled detrended fossil fuel CO_2 concentration with the annual mean subtracted, and C_M and Δ_M are the observed CO_2 concentration and $\Delta^{14}C$ in CO_2. $\delta\Delta_{ff,seas}$ was binned by month to compute monthly means and standard errors in the same manner as the observations.

[53] $\delta\Delta_{ff,seas}$ was also estimated for 16 models that participated in the Transcom 3 Experiment [*Gurney et al.*, 2002, 2003] in order to quantify the uncertainty in $\delta\Delta_{ff,seas}$ from different models' representations of atmospheric transport. Monthly mean fossil fuel CO_2 concentrations resulting from the transport of *Brenkert*'s [1998] pattern of aseasonal fossil fuel emissions for 1995 were detrended and used to calculate $\delta\Delta_{ff,seas}$. Our comparison of Transcom model results from 1995 to the TM3 model results from 2001–07 is reasonable since the amplitude of $\delta\Delta_{ff,seas}$ remained largely constant over 1992–2007 (Figure 6). Again we note that comparing the spread over different models may underestimate the transport uncertainty, due to biases in common model formulations or meteorological products.

Appendix B: Data Tables

[54] Measurements of $\Delta^{14}C$ in CO_2 samples collected by the Scripps CO_2 Program and measured at Lawrence Livermore National Laboratory are provided in Tables B1–B6. The CO_2 mole ratio and $\delta^{13}C$ listed are an average of all measurements with the same sample date. The $\delta^{13}C$ values footnoted with an "a" are estimates of $\delta^{13}C$ when measurements of $\delta^{13}C$ in concurrently sampled CO_2 were not available. CO_2 mole ratios were measured on the 'SIO 2008A' Calibration Scale. The SIO calibration scale for CO_2 is established by infrared and manometric analysis of primary reference gases [*Keeling et al.*, 2002]. The SIO calibration scale is tied to the historic CO_2 measurements at SIO and independent of the WMO scale since 1995. $\delta^{13}C$ values are relative to the international V-PDB standard and include the addition of a −0.112 ‰ offset for consistency with measurements performed at the Center for Isotope Research, University of Groningen, Netherlands. σ_{Tot} is the total measurement uncertainty in $\Delta^{14}C$. Flagged samples (16%) have been removed. $\Delta^{14}C$ measurements from La Jolla, California, USA are reported in the companion paper [*Graven et al.*, 2012].

Table B1. Measurements From Point Barrow, Alaska, USA

SIO ID	LLNL ID	Sample Date	CO_2 (ppm)	$\delta^{13}C$ (‰)	$\Delta^{14}C$ (‰)	σ_{Tot} (‰)
M99-002	126909	12-Jun-99	373.73	−8.453	91.8	1.7
M99-004	117889	03-Jul-99	362.60	−7.96[a]	98.8	1.7
M99-006	126930	15-Aug-99	353.65	−7.67[a]	91.6	1.7
M99-008	131097	25-Sep-99	365.99	−7.81[a]	93.3	1.7
M99-024	117888	22-Oct-99	364.99	−7.960	97.4	1.8
M99-025	131033	19-Nov-99	374.38	−8.15[a]	89.0	1.7
M99-027	117887	25-Dec-99	375.00	−8.420	87.6	1.7
M99-028	131125	29-Jan-00	373.47	−8.350	90.7	1.7
M99-029	126917	12-Feb-00	375.05	−8.427	85.7	1.7
M99-031	117886	09-Mar-00	373.80	−8.354	88.7	1.7
M01-030	131506	27-Jul-01	362.58	−7.638	79.8	1.7
M01-032	117892	01-Sep-01	363.19	−7.720	82.5	1.9
M01-046	131072	18-Oct-01	369.23	−8.12[a]	86.8	1.7
M01-102	131568	08-Dec-01	375.51	−8.351	80.0	1.7
M01-104	131058	16-Feb-02	377.17	−8.414	75.7	1.7
M01-130	117893	16-Mar-02	381.72	−8.51[a]	71.3	1.8
M01-163	131129	20-Apr-02	379.17	−8.452	72.8	1.7
M01-165	131537	28-May-02	378.48	−8.430	71.7	1.7
M01-193	124203	26-Jul-02	368.71	−7.84[a]	75.3	1.7
M01-221	117793	18-Oct-02	374.75	−8.07[a]	77.1	1.7
M01-267	117771	18-Nov-02	374.68	−8.225	80.4	2.8
M01-268	138082	30-Nov-02	376.97	−8.320	75.8	2.2
M01-269	117749	25-Dec-02	385.54	−8.37[a]	72.6	2.7
M01-298	117850	17-Jan-03	377.63	−8.354	68.4	2.7
M01-300	117810	24-Feb-03	383.83	−8.674	67.0	2.0
M01-322	117845	17-Mar-03	386.80	−8.53[a]	63.8	2.7
M01-340	117789	02-May-03	382.87	−8.57[a]	61.7	1.7
M01-343	117838	13-Jun-03	380.76	−8.523	69.1	2.7
M01-352	117851	12-Jul-03	369.90	−8.004	70.1	2.7
M01-353	117844	16-Aug-03	366.13	−7.68[a]	69.8	2.7
M01-385	117805	13-Sep-03	367.59	−7.806	71.5	1.7
M01-387	126998	10-Oct-03	371.84	−8.050	74.1	1.7
M01-453	126965	10-Jan-04	383.50	−8.601	70.0	1.7
M01-476	124202	13-Mar-04	381.81	−8.511	62.7	1.7
M01-478	128078	09-Apr-04	384.20	−8.551	64.1	1.7
M01-493	124196	07-May-04	383.22	−8.630	63.7	1.7
M01-511	128116	10-Jun-04	382.91	−8.481	62.6	1.7
M01-513	128091	01-Jul-04	374.59	−8.126	60.9	1.7
M01-530	124198	13-Aug-04	363.31	−7.55[a]	67.1	1.7
M01-556	126939	13-Sep-04	367.30	−7.738	63.5	1.7
M01-558	124187	07-Oct-04	371.42	−7.95[a]	67.2	1.7
M01-568	126988	12-Nov-04	380.83	−8.388	67.4	1.7
M01-641	128139	18-Feb-05	384.67	−8.539	62.7	1.7
M01-642	128151	25-Mar-05	385.79	−8.606	60.3	1.7
M01-659	128144	22-Apr-05	385.66	−8.614	59.7	1.7
M01-661	128100	20-May-05	385.36	−8.602	56.5	1.7
M01-682	128131	17-Jun-05	383.25	−8.463	57.9	1.7
M01-684	126974	22-Jul-05	373.55	−7.954	64.9	1.7
M01-727	128069	30-Sep-05	373.53	−7.904	61.4	1.7
M01-729	128286	24-Oct-05	377.67	−8.133	58.8	1.7
M01-757	128272	14-Dec-05	384.57	−8.444	56.1	1.7
M01-777	131550	20-Jan-06	386.34	−8.588	55.9	1.7
M01-792	131535	17-Feb-06	386.46	−8.555	52.9	1.7
M01-800	131050	17-Mar-06	387.28	−8.582	54.8	1.7
M01-814	131575	21-Apr-06	387.43	−8.591	49.1	1.7
M01-840	131111	26-May-06	389.43	−8.722	52.5	1.7
M01-841	131099	16-Jun-06	387.14	−8.559	55.4	1.7
M01-852	131139	28-Jul-06	369.31	−7.707	57.0	1.7
M01-882	131025	31-Aug-06	371.07	−7.793	53.3	1.7
M01-883	131516	22-Sep-06	374.70	−7.979	57.1	1.7
M01-894	131082	03-Nov-06	383.90	−8.368	61.1	1.7
M01-925	131562	15-Dec-06	388.00	−8.546	53.0	1.7
M07-013	138041	05-Jan-07	390.77	−8.713	48.2	2.2
M07-014	138034	09-Feb-07	388.79	−8.609	54.0	2.2
M07-035	138132	09-Mar-07	388.66	−8.589	50.5	2.2
M07-049	138083	06-Apr-07	390.13	−8.633	49.8	2.2
M07-050	138095	04-May-07	389.47	−8.602	52.2	2.2
M07-087	138064	08-Jun-07	387.94	−8.538	49.2	2.2
M07-099	138109	17-Aug-07	372.62	−7.708	51.5	2.2
M07-101	138097	07-Sep-07	376.11	−7.884	46.6	2.2
M08-021	141195	12-Oct-07	379.28	−8.20[a]	48.5	2.2
M08-022	141178	01-Nov-07	383.48	−8.20[a]	46.1	2.2
M08-023	141139	07-Dec-07	389.02	−8.522	49.1	2.2

[a]Estimated $\delta^{13}C$ values, when direct measurements were not available.

Table B2. Measurements From Kumukahi, Hawaii, USA

SIO ID	LLNL ID	Sample Date	CO_2 (ppm)	$\delta^{13}C$ (‰)	$\Delta^{14}C$ (‰)	σ_{Tot} (‰)
M01-028	128113	13-Aug-01	366.80	−7.830	81.3	1.7
M01-029	124155	04-Sep-01	368.28	−7.904	80.7	1.7
M01-056	128132	29-Oct-01	369.83	−8.022	77.6	1.7
M01-092	131124	19-Nov-01	372.75	−8.121	80.5	1.7
M01-095	126916	14-Jan-02	373.06	−8.153	81.9	1.7
M01-124	127002	19-Feb-02	373.97	−8.199	79.3	1.7
M01-128	126940	18-Mar-02	376.00	−8.311	72.4	1.7
M01-140	126972	15-Apr-02	375.37	−8.233	80.7	1.7
M01-142	131034	29-Apr-02	375.84	−8.246	74.8	1.7
M01-159	124156	13-May-02	376.51	−8.264	71.4	1.7
M01-177	128088	17-Jun-02	374.15	−8.147	74.3	1.7
M01-179	141174	01-Jul-02	373.80	−8.113	73.9	2.2
M01-181	128143	15-Jul-02	372.24	−8.029	79.0	1.7
M01-176	124154	12-Aug-02	368.80	−7.833	72.5	1.7
M01-210	117769	03-Sep-02	366.84	−7.800	80.8	2.7
M01-212	131522	16-Sep-02	366.81	−7.778	76.8	1.7
M01-214	117756	07-Oct-02	370.16	−7.943	79.5	2.8
M01-254	138060	18-Nov-02	372.47	−8.027	76.9	2.2
M01-256	117751	02-Dec-02	374.20	−8.157	67.8	2.8
M01-258	124145	16-Dec-02	376.86	−8.230	69.3	1.7
M01-284	117852	07-Jan-03	377.32	−8.269	66.4	3.0
M01-288	117753	03-Feb-03	377.70	−8.236	71.1	2.8
M01-307	117757	03-Mar-03	378.07	−8.286	70.5	2.7
M01-308	124138	17-Mar-03	377.54	−8.277	66.5	1.7
M01-324	124139	14-Apr-03	379.25	−8.333	67.0	1.7
M01-329	117781	03-Jun-03	380.17	−8.415	69.7	1.7
M01-364	128281	08-Sep-03	371.27	−7.924	69.4	1.7
M01-398	124143	14-Oct-03	373.10	−8.01[a]	71.4	1.7
M01-400	131599	10-Nov-03	374.78	−8.108	69.7	1.7
M01-441	131588	15-Dec-03	376.21	−8.174	68.7	1.7
M01-444	124144	12-Jan-04	377.33	−8.180	64.3	1.7
M01-445	128289	02-Feb-04	378.31	−8.256	64.0	1.7
M01-459	126994	01-Mar-04	378.23	−8.256	71.4	1.7
M01-485	131023	04-May-04	380.38	−8.303	67.4	1.7
M01-497	124140	01-Jun-04	381.18	−8.325	64.9	1.7
M01-514	128282	06-Jul-04	378.66	−8.214	68.5	1.7
M01-545	128067	16-Aug-04	373.69	−7.974	67.3	1.7
M01-547	131584	13-Sep-04	374.94	−8.018	66.3	1.7
M01-559	128124	04-Oct-04	374.85	−8.048	63.7	1.7
M01-596	128068	15-Nov-04	377.95	−8.189	60.3	1.7
M01-599	128288	21-Dec-04	377.88	−8.153	60.9	1.7
M01-614	131593	18-Jan-05	378.50	−8.130	68.0	1.7
M01-624	131603	22-Feb-05	382.56	−8.351	63.1	1.7
M01-636	128275	28-Mar-05	382.22	−8.402	57.5	1.7
M01-639	128153	25-Apr-05	383.63	−8.445	60.8	1.7
M01-665	126947	23-May-05	384.23	−8.384	55.3	1.7
M01-688	128077	20-Jun-05	382.28	−8.346	56.0	1.7
M01-692	131594	19-Jul-05	377.83	−8.141	60.2	1.7
M01-717	126920	06-Sep-05	375.95	−7.978	62.4	1.7
M01-724	126908	11-Oct-05	376.62	−8.043	63.6	1.7
M01-749	128269	07-Nov-05	378.68	−8.126	57.9	1.7
M01-769	126968	09-Jan-06	381.82	−8.255	56.8	1.7
M01-781	128102	17-Jan-06	382.33	−8.280	56.1	1.7
M01-793	131102	21-Feb-06	383.35	−8.344	54.6	1.7
M01-809	131133	20-Mar-06	383.00	−8.293	55.7	1.7
M01-812	131057	17-Apr-06	384.73	−8.374	59.8	1.7
M01-829	131107	15-May-06	387.21	−8.552	53.4	1.7
M01-832	131073	12-Jun-06	385.06	−8.355	61.8	1.7
M01-854	131576	10-Jul-06	382.41	−8.262	56.9	1.7
M01-858	131503	07-Aug-06	376.69	−7.971	56.2	1.7
M01-879	131567	11-Sep-06	377.60	−7.984	58.7	1.7
M01-890	131080	09-Oct-06	378.08	−8.029	59.7	1.7
M01-920	131548	13-Nov-06	379.62	−8.138	56.9	1.7
M01-922	131530	11-Dec-06	382.57	−8.253	52.9	1.7
M07-010	138089	16-Jan-07	383.41	−8.259	51.7	2.2
M07-027	138066	19-Mar-07	384.54	−8.291	56.5	2.2
M07-046	138113	16-Apr-07	386.63	−8.427	49.3	2.2
M07-056	138053	14-May-07	387.04	−8.408	51.5	2.2
M07-070	138042	18-Jun-07	386.19	−8.382	55.2	2.2
M07-094	138139	23-Jul-07	381.88	−8.204	52.3	2.2
M07-097	138108	20-Aug-07	375.19	−7.823	53.5	2.2
M07-111	138038	17-Sep-07	379.62	−8.00[a]	49.9	2.2
M07-126	141134	16-Oct-07	381.91	−8.10[a]	50.7	2.2
M07-129	141116	19-Nov-07	382.52	−8.160	49.5	2.2
M08-030	141198	17-Dec-07	384.50	−8.270	44.3	2.2

[a]Estimated $\delta^{13}C$ values, when direct measurements were not available.

Table B3. Measurements From Mauna Loa, Hawaii, USA

SIO ID	LLNL ID	Sample Date	CO_2 (ppm)	$\delta^{13}C$ (‰)	$\Delta^{14}C$ (‰)	σ_{Tot} (‰)
M01-024	124190	22-Aug-01	369.25	−7.937	85.9	1.7
M01-027	104521	12-Sep-01	368.90	−7.935	81.9	2.2
M01-040	131518	26-Sep-01	367.58	−7.887	85.2	1.7
M01-043	104522	17-Oct-01	368.09	−7.893	79.6	2.2
M01-058	124362	07-Nov-01	369.05	−7.959	86.0	1.7
M01-059	104523	14-Nov-01	369.81	−7.990	78.9	2.2
M01-083	104525	16-Jan-02	372.37	−8.090	79.3	2.2
M01-108	104526	13-Feb-02	372.80	−8.094	79.1	2.2
M01-110	124349	01-Mar-02	372.91	−8.132	80.0	1.7
M01-118	104527	13-Mar-02	374.09	−8.174	77.4	2.2
M01-122	104528	10-Apr-02	374.18	−8.137	77.1	2.2
M01-144	124352	24-Apr-02	375.44	−8.231	78.7	1.7
M01-146	104529	08-May-02	374.21	−8.103	73.1	2.2
M01-154	124353	29-May-02	376.09	−8.252	78.0	1.7
M01-183	124355	07-Aug-02	371.05	−7.985	74.0	1.7
M01-185	104532	21-Aug-02	371.72	−8.023	77.8	2.2
M01-200	124359	04-Sep-02	369.34	−7.904	78.6	1.7
M01-202	117800	18-Sep-02	369.79	−7.926	76.0	1.7
M01-206	117759	16-Oct-02	371.71	−7.982	73.6	2.7
M01-231	117747	13-Nov-02	372.05	−8.000	75.5	2.7
M01-251	117809	18-Dec-02	373.67	−8.071	75.6	1.7
M01-265	117799	15-Jan-03	374.11	−8.085	76.9	1.7
M01-304	117784	19-Mar-03	376.40	−8.236	72.4	1.7
M01-317	117746	16-Apr-03	378.47	−8.344	71.7	2.8
M01-321	117773	14-May-03	377.29	−8.242	72.3	2.7
M01-337	124360	28-May-03	379.17	−8.316	72.1	1.7
M01-338	131566	04-Jun-03	378.45	−8.264	73.3	1.7
M01-348	117770	16-Jul-03	376.11	−8.221	71.7	2.7
M01-351	117755	13-Aug-03	374.80	−8.062	73.6	3.0
M01-371	126913	10-Sep-03	372.58	−8.042	73.7	1.7
M01-390	124363	01-Oct-03	373.29	−8.033	72.5	1.7
M01-394	124342	29-Oct-03	373.19	−8.017	70.5	1.7
M01-410	126905	07-Jan-04	375.88	−8.107	70.9	1.7
M01-448	124204	04-Feb-04	377.40	−8.197	69.6	1.7
M01-451	126971	01-Mar-04	377.82	−8.214	72.8	1.7
M01-471	124344	24-Mar-04	378.53	−8.241	68.0	1.7
M01-486	124188	28-Apr-04	380.28	−8.355	67.9	1.7
M01-488	124191	12-May-04	379.89	−8.457	67.2	1.7
M01-505	124194	16-Jun-04	379.52	−8.304	66.2	1.7
M01-522	126950	14-Jul-04	376.02	−8.140	64.7	1.7
M01-527	124343	18-Aug-04	375.33	−8.079	68.3	1.7
M01-535	128107	15-Sep-04	374.06	−7.985	68.0	1.7
M01-552	126918	13-Oct-04	374.15	−8.034	62.9	1.7
M01-571	124346	17-Nov-04	376.48	−8.090	66.7	1.7
M01-572	124347	24-Nov-04	376.41	−8.131	65.8	1.7
M01-590	124348	08-Dec-04	377.36	−8.138	64.8	1.7
M01-595	128090	12-Jan-05	378.85	−8.247	61.6	1.7
M01-618	128103	16-Feb-05	380.16	−8.288	62.3	1.7
M01-630	128148	16-Mar-05	381.88	−8.318	64.0	1.7
M01-634	128098	13-Apr-05	381.49	−8.696	61.2	1.7
M01-654	128082	11-May-05	382.06	−8.282	62.2	1.7
M01-674	128140	13-Jul-05	381.39	−8.263	62.3	1.7
M01-702	128128	10-Aug-05	378.05	−8.168	62.0	1.7
M01-709	127001	14-Sep-05	376.12	−8.039	65.2	1.7
M01-732	131531	26-Oct-05	377.19	−8.095	62.4	1.7
M01-754	138136	30-Nov-05	378.68	−8.138	65.0	2.2
M01-756	126964	14-Dec-05	379.41	−8.209	63.1	1.7
M01-773	128075	11-Jan-06	381.04	−8.259	56.8	1.7
M01-784	131122	08-Feb-06	381.99	−8.217	62.2	1.7
M01-796	131113	08-Mar-06	382.79	−8.313	56.8	1.7
M01-802	131132	05-Apr-06	384.06	−8.397	57.2	1.7
M01-816	131065	10-May-06	385.34	−8.458	60.5	1.7
M01-836	131504	14-Jun-06	383.9	−8.344	58.8	1.7
M01-846	131098	12-Jul-06	381.75	−8.277	56.0	1.7
M01-864	131024	16-Aug-06	379.97	−8.143	60.1	1.7
M01-869	131061	20-Sep-06	378.31	−8.107	59.2	1.7
M01-887	131096	18-Oct-06	379.30	−8.126	57.0	1.7
M01-910	131037	15-Nov-06	379.82	−8.112	57.2	1.7
M01-914	131539	13-Dec-06	380.93	−8.184	55.3	1.7
M07-018	138127	14-Feb-07	384.58	−8.317	60.4	2.2
M07-031	138055	13-Mar-07	384.49	−8.387	53.6	2.2
M07-044	138118	18-Apr-07	387.57	−8.473	53.3	2.2
M07-059	138037	16-May-07	386.24	−8.388	53.0	2.2
M07-068	138090	13-Jun-07	386.50	−8.346	50.8	2.2
M07-076	138103	18-Jul-07	384.33	−8.24[a]	55.0	2.2
M07-104	138120	13-Sep-07	378.92	−8.10[a]	53.9	2.2
M07-120	141155	17-Oct-07	380.86	−8.109	49.7	2.2
M07-124	141147	15-Nov-07	382.01	−8.161	49.7	2.2
M08-026	141172	13-Dec-07	383.62	−8.218	52.8	2.2

[a]Estimated $\delta^{13}C$ values, when direct measurements were not available.

Table B4. Measurements From Cape Matatula, American Samoa

SIO ID	LLNL ID	Sample Date	CO_2 (ppm)	$\delta^{13}C$ (‰)	$\Delta^{14}C$ (‰)	σ_{Tot} (‰)
M01-049	117880	25-Sep-01	370.04	−7.988	85.3	1.7
M01-084	117881	29-Oct-01	370.06	−7.940	83.5	1.7
M01-085	104537	07-Nov-01	370.12	−8.014	85.3	2.2
M01-112	117882	29-Jan-02	370.53	−7.967	83.0	1.7
M01-132	104541	12-Mar-02	372.16	−8.029	83.8	2.2
M01-136	104542	09-Apr-02	370.71	−7.999	83.0	2.2
M01-137	117883	19-Apr-02	370.50	−7.999	79.9	2.0
M01-150	104543	14-May-02	370.63	−7.966	81.9	2.2
M01-171	104544	18-Jun-02	371.72	−8.023	78.4	2.2
M01-188	104545	19-Jul-02	371.48	−8.013	78.8	2.2
M01-189	117884	23-Jul-02	371.83	−8.032	79.6	1.7
M01-196	104546	14-Aug-02	372.19	−8.037	77.4	2.2
M01-197	117885	26-Aug-02	372.19	−8.023	78.0	1.8
M01-225	131131	29-Oct-02	372.89	−8.041	77.5	1.7
M01-228	117807	19-Nov-02	373.21	−8.061	79.3	1.7
M01-271	131064	03-Dec-02	373.85	−8.095	79.7	1.7
M01-275	131501	31-Dec-02	372.94	−8.072	79.9	1.7
M01-293	117767	18-Feb-03	373.26	−8.043	78.4	2.7
M01-311	117766	11-Mar-03	374.76	−8.082	77.7	2.8
M01-313	126984	11-Apr-03	374.88	−8.121	79.5	1.7
M01-315	131062	22-Apr-03	373.03	−8.020	79.3	1.7
M01-331	117840	23-May-03	373.28	−8.077	79.2	2.7
M01-359	117765	16-Jul-03	373.44	−8.10[a]	73.6	2.7
M01-365	117891	30-Jul-03	374.37	−8.086	79.1	1.7
M01-375	138052	03-Sep-03	374.17	−8.069	68.9	2.2
M01-377	126942	16-Sep-03	374.25	−8.057	73.0	1.7
M01-383	141125	28-Oct-03	374.19	−8.086	73.8	2.2
M01-434	126935	17-Nov-03	374.55	−8.106	69.4	1.7
M01-438	126914	16-Dec-03	375.50	−8.059	75.7	1.7
M01-465	126991	11-Feb-04	376.21	−8.076	74.5	1.7
M01-468	117871	09-Mar-04	376.41	−8.096	72.8	2.3
M01-480	117872	13-Apr-04	376.01	−8.104	71.0	1.8
M01-482	117873	27-Apr-04	375.14	−8.072	71.8	1.7
M01-501	117874	18-May-04	375.51	−8.074	71.3	2.0
M01-509	128277	16-Jun-04	376.33	−8.088	71.2	1.7
M01-518	128118	14-Jul-04	375.65	−8.064	68.8	1.7
M01-540	117875	09-Aug-04	376.22	−8.108	68.7	1.8
M01-544	126931	07-Sep-04	375.85	−8.085	65.1	1.7
M01-564	117877	09-Nov-04	375.98	−8.010	67.9	1.7
M01-566	117878	24-Nov-04	376.19	−8.123	68.0	1.7
M01-603	128072	05-Jan-05	377.67	−8.132	68.3	1.7
M01-617	126963	10-Feb-05	377.39	−8.128	67.9	1.7
M01-646	126959	11-Apr-05	377.93	−8.078	64.1	1.7
M01-650	128137	12-May-05	379.39	−8.155	68.7	1.7
M01-680	128063	17-Jun-05	377.80	−8.140	65.0	1.7
M01-695	128147	18-Jul-05	378.42	−8.159	68.5	1.7
M01-699	128094	17-Aug-05	378.05	−8.096	63.5	1.7
M01-720	128106	13-Sep-05	378.34	−8.108	62.9	1.7
M01-734	128125	12-Oct-05	378.17	−8.103	63.6	1.7
M01-760	128156	17-Nov-05	378.97	−8.127	65.9	1.7
M01-763	126997	13-Dec-05	378.08	−8.145	66.0	1.7
M01-775	128081	04-Jan-06	379.89	−8.119	62.5	1.7
M01-788	131081	18-Feb-06	380.87	−8.161	67.4	1.7
M01-808	131032	27-Mar-06	378.75	−8.143	63.8	1.7
M01-823	131103	25-Apr-06	378.72	−8.138	62.0	1.7
M01-843	131510	28-Jun-06	380.05	−8.159	62.7	1.7
M01-860	131060	28-Jul-06	379.95	−8.170	59.8	1.7
M01-871	131121	28-Aug-06	379.94	−8.142	57.6	1.7
M01-875	131114	25-Sep-06	379.69	−8.121	60.9	1.7
M01-898	131560	23-Oct-06	379.83	−8.150	59.3	1.7
M01-929	131049	29-Dec-06	381.64	−8.134	58.7	1.7
M07-037	138035	27-Feb-07	382.55	−8.190	50.8	2.2
M07-040	138044	23-Mar-07	382.25	−8.126	52.8	2.2
M07-063	138131	30-May-07	382.24	−8.136	56.0	2.2
M07-080	138102	28-Jun-07	380.88	−8.107	56.8	2.2
M07-090	138033	27-Jul-07	382.16	−8.152	53.5	2.2
M07-107	138091	22-Aug-07	381.98	−8.138	55.4	2.2
M07-109	138074	25-Sep-07	382.36	−8.115	52.0	2.2
M07-117	141168	23-Oct-07	382.37	−8.121	51.5	2.2
M08-034	141130	16-Nov-07	382.55	−8.082	51.6	2.2
M08-035	141122	28-Nov-07	382.84	−8.134	51.9	2.2
M08-037	141150	19-Dec-07	383.16	−8.098	48.1	2.2

[a]Estimated $\delta^{13}C$ values, when direct measurements were not available.

Table B5. Measurements From Palmer Station, Antarctica

SIO ID	LLNL ID	Sample Date	CO_2 (ppm)	$\delta^{13}C$ (‰)	$\Delta^{14}C$ (‰)	σ_{Tot} (‰)
PSA-01A	131523	10-Mar-05	375.18	−8.098	64.6	1.7
PSA-03A	131120	19-May-05	376.23	−8.107	59.5	1.7
PSA-04A	131529	03-Jul-05	377.00	−8.119	60.5	1.7
PSA-05A	131557	23-Sep-05	378.06	−8.147	58.1	1.7
PSA-06A	131086	20-Oct-05	377.90	−8.128	65.3	1.7
PSA-07A	131572	30-Nov-05	377.26	−8.148	57.3	1.7
PSA-08A	131030	12-Dec-05	377.55	−8.153	58.2	1.7
PSA-09A	131507	30-Dec-05	377.36	−8.099	58.6	1.7
PSA-10A	131041	16-Jan-06	377.47	−8.139	61.7	1.7
PSA-11A	131140	06-Feb-06	377.14	−8.099	62.0	1.7
PSA-12A	131563	02-Mar-06	377.57	−8.087	62.4	1.7
PSA-13A	131135	20-Mar-06	384.73	−8.098	61.9	1.7
PSA-14A	131084	17-Apr-06	378.08	−8.072	66.2	1.7
PSA-15A	131512	29-Apr-06	378.04	−8.093	59.0	1.7
PSA-16A	131101	28-Jun-06	378.97	−8.116	60.7	1.7
PSA-17A	131028	10-Jul-06	378.69	−8.130	57.6	1.7
PSA-18A	131540	24-Jul-06	378.94	−8.158	57.6	1.7
PSA-19A	131074	07-Aug-06	379.14	−8.185	60.6	1.7
PSA-20A	131558	07-Nov-06	379.73	−8.163	55.7	1.7
PSA-21A	131579	02-Dec-06	379.76	−8.174	54.5	1.7
PSA-23A	138040	02-Jan-07	378.93	−8.159	58.0	2.2
PSA-24A	138107	28-Feb-07	378.94	−8.132	57.7	2.2
PSA-25A	138047	27-Mar-07	379.43	−8.145	54.0	2.2
PSA-26A	138124	15-Apr-07	379.67	−8.102	60.5	2.2
PSA-27A	138088	22-May-07	380.64	−8.148	56.0	2.2
PSA-28A	138073	06-Jun-07	380.40	−8.149	54.1	2.2
PSA-29A	138111	03-Jul-07	380.59	−8.14[a]	52.9	2.2
PSA-30A	141166	18-Jul-07	380.96	−8.123	52.5	2.2
PSA-32A	138117	03-Aug-07	381.71	−8.145	51.9	2.2
PSA-31A	141140	04-Aug-07	381.14	−8.153	53.4	2.2
PSA-33A	138096	11-Sep-07	381.68	−8.188	55.5	2.2

[a]Estimated $\delta^{13}C$ values, when direct measurements were not available.

Table B6. Measurements From the South Pole, Antarctica

SIO ID	LLNL ID	Sample Date	CO_2 (ppm)	$\delta^{13}C$ (‰)	$\Delta^{14}C$ (‰)	σ_{Tot} (‰)
M99-010	131574	16-Feb-99	364.76	−8.034	96.0	1.7
M99-011	131559	01-Mar-99	364.81	−7.982	97.9	1.7
M99-012	117824	01-May-99	364.97	−7.973	92.6	2.7
M99-013	126962	15-Jul-99	365.68	−7.999	97.1	1.7
M99-014	128152	17-Aug-99	365.95	−7.980	93.0	1.7
M99-016	128099	16-Sep-99	366.24	−7.983	89.4	1.7
M99-018	126946	17-Oct-99	366.63	−8.024	86.3	1.7
M99-020	126911	19-Nov-99	369.52	−8.01[a]	92.4	1.7
M99-022	131127	23-Jan-00	366.40	−8.007	93.2	1.7
M01-001	128284	18-Feb-00	366.48	−8.011	93.0	1.7
M01-004	128280	15-Apr-00	366.51	−8.010	89.8	1.7
M01-008	117826	16-Jun-00	366.73	−7.988	86.6	2.7
M01-010	128071	15-Jul-00	367.06	−7.990	84.4	1.7
M01-013	126985	02-Sep-00	367.60	−8.005	88.6	1.7
M01-015	117864	01-Oct-00	367.69	−7.998	87.6	1.7
M01-017	128290	01-Nov-00	367.88	−7.998	86.2	1.7
M01-019	117827	02-Dec-00	367.79	−7.982	86.3	2.8
M01-021	131040	15-Jan-01	367.82	−7.980	92.2	1.7
M01-065	128064	15-Feb-01	367.11	−7.983	88.7	1.7
M01-067	128270	15-Mar-01	367.05	−7.966	81.4	1.7
M01-069	117828	16-Apr-01	367.35	−7.958	85.7	2.7
M01-071	126996	15-May-01	367.61	−7.969	88.3	1.7
M01-074	131509	01-Jul-01	367.97	−7.976	87.9	1.7
M01-078	117830	15-Sep-01	369.35	−7.997	78.8	3.1
M01-100	138094	02-Jan-02	369.28	−8.028	75.6	2.2
M01-233	117831	13-Feb-02	369.50	−8.010	75.8	2.8
M01-240	117853	01-Jul-02	370.62	−7.985	78.6	2.8
M01-242	117772	01-Aug-02	371.16	−8.031	76.6	2.7
M01-244	117752	02-Sep-02	371.48	−8.025	73.5	2.6
M01-259	117745	02-Nov-02	371.82	−8.057	79.3	2.7
M01-261	117795	03-Dec-02	371.72	−8.045	76.3	1.7

Table B6. (continued)

SIO ID	LLNL ID	Sample Date	CO_2 (ppm)	$\delta^{13}C$ (‰)	$\Delta^{14}C$ (‰)	σ_{Tot} (‰)
M01-412	117761	01-Feb-03	371.73	−8.009	73.2	2.7
M01-415	138071	17-Mar-03	371.80	−8.017	72.9	2.2
M01-416	117836	01-Apr-03	371.83	−8.108	75.3	2.7
M01-418	117768	01-May-03	372.06	−8.034	69.0	2.8
M01-420	117841	01-Jun-03	372.36	−8.034	74.0	2.7
M01-422	117806	02-Jul-03	372.72	−8.062	72.0	1.7
M01-424	117783	01-Aug-03	373.08	−8.054	72.9	1.7
M01-426	128123	01-Sep-03	373.79	−8.090	66.8	1.7
M01-428	131544	01-Oct-03	373.80	−8.073	70.9	1.7
M01-430	117832	16-Nov-03	373.65	−8.085	68.9	2.7
M01-456	128149	03-Jan-04	373.67	−8.066	72.9	1.7
M01-458	131109	01-Feb-04	373.37	−8.094	72.0	1.7
M01-574	117833	03-Mar-04	373.94	−8.059	71.2	2.8
M01-575	131088	02-Apr-04	373.75	−8.136	76.8	1.7
M01-580	126934	18-Jun-04	374.54	−8.109	64.4	1.7
M01-581	128104	15-Jul-04	374.84	−8.144	65.9	1.7
M01-583	117867	16-Aug-04	375.33	−8.159	65.2	1.7
M01-585	126993	18-Sep-04	375.5	−8.112	67.9	1.7
M01-587	117868	17-Oct-04	375.56	−8.142	70.5	2.1
M01-588	117868	02-Nov-04	375.63	−8.126	69.4	2.6
M01-611	128273	01-Jan-05	375.43	−8.117	67.4	1.7
M01-736	128285	02-Feb-05	374.95	−8.121	65.8	1.7
M01-738	126921	15-Mar-05	375.60	−8.090	66.6	1.7
M01-740	126970	02-May-05	376.18	−8.162	67.3	1.7
M01-741	126944	01-Jun-05	376.22	−8.156	59.0	1.7
M01-743	128127	30-Jun-05	376.71	−8.166	58.7	1.7
M01-744	128079	15-Sep-05	377.69	−8.159	60.9	1.7
M01-746	131026	19-Oct-05	378.03	−8.165	66.2	1.7
M01-765	128136	15-Nov-05	377.75	−8.205	64.6	1.7
M01-766	128276	16-Dec-05	377.03	−8.181	64.6	1.7
M01-778	131136	15-Jan-06	377.80	−8.197	65.8	1.7
M01-915	131089	15-Feb-06	377.43	−8.136	64.9	1.7
M01-899	131052	15-Apr-06	378.58	−8.142	62.6	1.7
M01-901	131532	15-May-06	377.91	−8.157	54.3	1.7
M01-903	131520	01-Jul-06	378.61	−8.158	65.6	1.7
M01-905	131565	01-Aug-06	379.03	−8.173	59.6	1.7
M01-907	131106	19-Sep-06	379.34	−8.163	58.0	1.7
M01-908	131071	18-Oct-06	379.24	−8.194	61.3	1.7
M01-909	131514	15-Nov-06	379.25	−8.182	62.9	1.7
M07-001	138054	01-Jan-07	379.32	−8.148	53.4	2.2
M07-003	138084	01-Feb-07	379.28	−8.131	51.9	2.2
M08-002	138081	01-Mar-07	379.25	−8.134	52.5	2.2
M08-004	138043	03-Apr-07	379.47	−8.130	57.3	2.2
M08-006	138123	01-May-07	379.86	−8.144	53.8	2.2
M08-008	138098	01-Jun-07	380.16	−8.157	54.8	2.2
M08-010	138067	01-Jul-07	380.44	−8.157	58.2	2.2
M08-012	138119	01-Aug-07	380.94	−8.202	55.7	2.2
M08-014	138137	03-Sep-07	381.38	−8.177	58.5	2.2
M08-018	141200	01-Nov-07	381.64	−8.252	57.6	2.2
M08-020	141149	04-Dec-07	381.60	−8.189	54.3	2.2

[a]Estimated $\delta^{13}C$ values, when direct measurements were not available.

[55] **Acknowledgments.** The air sampling and CO_2 extractions were supported by a grant from BP, by the National Science Foundation (NSF) under grant ATM-0632770, the U.S. Department of Energy (DOE) under grant DE-FG02-07ER64362 as well as by previous awards from NSF and DOE. This work was performed in part under the auspices of the U.S. Department of Energy by Lawrence Livermore National Laboratory under contract W-7405-Eng-48 and DE-AC52-07NA27344. Radiocarbon analyses were funded by grants from NOAA's Office of Global Programs (NA05OAR4311166) and LLNL's Directed Research and Development program (06-ERD-031) to T.P.G. H.D.G. received support from the UC Office of the President and a NASA ESS Fellowship. H.D.G. also thanks Nicolas Gruber for support and helpful discussions. Alane Bollenbacher conducted CO_2 and stable isotope analyses. We thank the anonymous reviewers and Jocelyn Turnbull for helpful comments and Ingeborg Levin for sharing recent $\Delta^{14}C$ data from Jungfraujoch. We acknowledge the work of the Transcom modelers and assistance from Christian Rödenbeck with the TM3 Model. This research was also presented in H.D.G.'s doctoral dissertation at the University of California, San Diego, USA, 2008.

References

Andres, R. J., G. Marland, I. Fung, and E. Matthews (1996), A 1° × 1° distribution of carbon dioxide emissions from fossil fuel consumption and cement manufacture, 1950–1990, *Global Biogeochem. Cycles*, *10*, 419–429.

Andres, R. J., J. S. Gregg, L. Losey, G. Marland, and T. A. Boden (2011), Monthly, global emissions of carbon dioxide from fossil fuel consumption, *Tellus, Ser. B*, *63*, 309–327.

Appenzeller, C., J. R. Holton, and K. H. Rosenlof (1996), Seasonal variation of mass transport across the tropopause, *J. Geophys. Res.*, *101*(D10), 15,071–15,078.

Blasing, T. J., C. T. Broniak, and G. Marland (2004), Estimates of monthly carbon dioxide emissions and associated $\delta^{13}C$ values from fossil-fuel consumption in the USA, in *Trends: A Compendium of Data on Global Change*, Carbon Dioxide Inf. Anal. Cent., Oak Ridge Natl. Lab., U.S. Dep. of Energy, Oak Ridge, Tenn., http://cdiac.ornl.gov/trends/emis_mon/emis_mon_co2.html

Brenkert, A. (1998), Carbon dioxide emission estimates from fossil-fuel burning, hydraulic cement production, and gas flaring for 1995 on a one degree grid cell basis, *NDP 058A*, Carbon Dioxide Inf. Anal. Cent., Oak Ridge Natl. Lab., U.S. Dep. of Energy, Oak Ridge, Tenn. [Available at http://cdiac.esd.ornl.gov/epubs/ndp/ndp058a/ndp058a.html.]

Broecker, W. S., T. H. Peng, G. Ostlund, and M. Stuiver (1985), The distribution of bomb radiocarbon in the ocean, *J. Geophys. Res.*, *90*(C4), 6953–6970.

Canadell, J., et al. (2007), Contributions to accelerating atmospheric CO_2 growth from economic activity, carbon intensity, and efficiency of natural sinks, *Proc. Natl. Acad. Sci., U. S. A.*, *104*(47), 18,866–18,870.

Cantrell, C. A. (2008), Technical Note: Review of methods for linear least-squares fitting of data and application to atmospheric chemistry problems, *Atmos. Chem. Phys.*, *8*, 5477–5487.

Conway, T. J., and P. Tans (2004), Atmospheric carbon dioxide mixing ratios from the NOAA CMDL Carbon Cycle Cooperative Global Air Sampling Network (2004), in *Trends: A Compendium of Data on Global Change*, Carbon Dioxide Inf. Anal. Cent., Oak Ridge Natl. Lab., U.S. Dep. of Energy, Oak Ridge, Tenn., ftp://cdiac.ornl.gov/pub/ndp005/README_co2.html

Cristofanelli, P., P. Bonasoni, L. Tositti, U. Bonafe, F. Calzolari, F. Evangelisti, S. Sandrini, and A. Stohl (2006), A 6-year analysis of stratospheric intrusions and their influence on ozone at Mt. Cimone (2165 m above sea level), *J. Geophys. Res.*, *111*(D3), D03306, doi:10.1029/2005JD006553.

Currie, K. I., G. Brailsford, S. Nichol, A. Gomez, R. Sparks, K. R. Lassey, and K. Riedel (2009), Tropospheric $^{14}CO_2$ at Wellington, New Zealand: the world's longest record, *Biogeochemistry*, *104*(1–3), 5–22, doi:10.1007/s10533-009-9352-6.

Erickson, D. J., III, R. T. Mills, J. Gregg, T. J. Blasing, F. M. Hoffman, R. J. Andres, M. Devries, Z. Zhu, and S. R. Kawa (2008), An estimate of monthly global emissions of anthropogenic CO_2: Impact on the seasonal cycle of atmospheric CO_2, *J. Geophys. Res.*, *113*, G01023, doi:10.1029/2007JG000435.

Gettelman, A., and A. H. Sobel (2000), Direct diagnoses of stratosphere-troposphere exchange, *J. Atmos. Sci.*, *57*(1), 3–16.

Graven, H. D. (2008), Advancing the use of radiocarbon in studies of global and regional carbon cycling with high precision measurements of ^{14}C in CO_2 from the Scripps CO_2 Program, Ph.D. thesis, Scripps Inst. of Oceanogr., Univ. of Calif., San Diego, La Jolla.

Graven, H. D., and N. Gruber (2011), Continental-scale enrichment of atmospheric $^{14}CO_2$ from the nuclear power industry: Potential impact on the estimation of fossil fuel-derived CO_2, *Atmos. Chem. Phys.*, *11*, 12,339–12,349, doi:10.5194/acp-11-12339-2011.

Graven, H. D., T. P. Guilderson, and R. F. Keeling (2007), Methods for high-precision ^{14}C AMS measurement of atmospheric CO_2 at LLNL, *Radiocarbon*, *49*, 349–356.

Graven, H. D., T. P. Guilderson, and R. F. Keeling (2012), Observations of radiocarbon in CO_2 at La Jolla, California, USA 1992–2007: Analysis of the long-term trend, *J. Geophys. Res.*, *117*, D02303, doi:10.1029/2011JD016533.

Gurney, K. R., R. M. Law, P. J. Rayner, and A. S. Denning (2000), TransCom 3 experimental protocol, *Pap. 707*, Dep. of Atmos. Sci., Colo. State Univ., Fort Collins.

Gurney, K. R., et al. (2002), Towards robust regional estimates of CO_2 sources and sinks using atmospheric transport models, *Nature*, *415*, 626–630.

Gurney, K. R., et al. (2003), TransCom 3 CO_2 inversion intercomparison: 1. Annual mean control results and sensitivity to transport and prior flux information, *Tellus, Ser. B*, *55*, 555–579.

Gurney, K. R., Y. H. Chen, T. Maki, S. R. Kawa, A. Andrews, and Z. Zhu (2005), Sensitivity of atmospheric CO_2 inversions to seasonal and

interannual variations in fossil fuel emissions, *J. Geophys. Res.*, *110*, D10308, doi:10.1029/2004JD005373.
Heimann, M., and S. Korner (2003), The Global Atmospheric Tracer Model TM3, Model description and users manual release 3.8a, *Tech. Rep. 5*, Max Planck Inst. for Biogeochem., Jena, Germany.
Hesshaimer, V., M. Heimann, and I. Levin (1994), Radiocarbon evidence for a smaller oceanic carbon dioxide sink than previously believed, *Nature*, *370*(6486), 201–203.
James, P., A. Stohl, C. Forster, S. Eckhardt, P. Seibert, and A. Frank (2003), A 15-year climatology of stratosphere-troposphere exchange with a Lagrangian particle dispersion model: 2 Mean climate and seasonal variability, *J. Geophys. Res.*, *108*(D12), 8522, doi:10.1029/2002JD002639.
Jenkins, W. J., K. L. Elder, A. P. McNichol, and K. von Reden (2010), The passage of the bomb radiocarbon pulse into the Pacific Ocean, *Radiocarbon*, *52*(2–3), 1182–1190.
Jöckel, P., and C. A. M. Brenninkmeijer (2002), The seasonal cycle of cosmogenic ^{14}CO at the surface level: A solar cycle adjusted, zonal average climatology based on observations, *J. Geophys. Res.*, *107*(D22), 4656, doi:10.1029/2001JD001104.
Jöckel, P., C. A. M. Brenninkmeijer, M. G. Lawrence, A. B. M. Jeuken, and P. F. J. van Velthoven (2002), Evaluation of stratosphere-troposphere exchange and the hydroxyl radical distribution using observations of cosmogenic ^{14}CO, *J. Geophys. Res.*, *107*(D20), 4446, doi:10.1029/2001JD001324.
Kalnay, E., et al. (1996), The NCEP/NCAR 40-Year Reanalysis Project, *Bull. Am. Meteorol. Soc.*, *77*(3), 437–472.
Keeling, C. D., P. R. Guenther, G. Emanuele, A. Bollenbacher, and D. J. Moss (2002), Scripps reference gas calibration system for carbon dioxide-in-nitrogen and carbon dioxide-in-air standards: Revision of 1999, a report prepared for the Global Environmental Monitoring Program of the World Meteorological Organization, report, 83 pp., World Meteorol. Org., Geneva.
Keeling, C. D., S. C. Piper, R. B. Bacastow, M. Wahlen, T. P. Whorf, M. Heimann, and H. A. Meijer (2005), Atmospheric CO_2 and $^{13}CO_2$ exchange with the terrestrial biosphere and oceans from 1978 to 2000: Observations and carbon cycle implications, in *A History of Atmospheric CO_2 and Its Effects on Plants, Animals and Ecosystems*, edited by J. R. Ehleringer, T. E. Cerling, and M. D. Dearing, pp. 83–113, Springer, New York.
Keeling, R. F., A. C. Manning, E. M. McEvoy, and S. R. Shertz (1998a), Methods for measuring changes in atmospheric O_2 concentration and their application in Southern Hemisphere air, *J. Geophys. Res.*, *103*(D3), 3381–3397.
Keeling, R. F., B. B. Stephens, R. G. Najjar, S. C. Doney, D. Archer, and M. Heimann (1998b), Seasonal variations in the atmospheric O_2/N_2 ratio in relation to the kinetics of air-sea gas exchange, *Global Biogeochem. Cycles*, *12*(1), 141–163.
Key, R. M., et al. (2004), A global ocean carbon climatology: Results from Global Data Analysis Project (GLODAP), *Global Biogeochem. Cycles*, *18*, GB4031, doi:10.1029/2004GB002247.
Kjellström, E., J. Feichter, and G. Hoffman (2000), Transport of SF_6 and $^{14}CO_2$ in the atmospheric general circulation model ECHAM 4, *Tellus, Ser. B*, *52*(1), 1–18.
Lal, D., and Rama (1966), Characteristics of global tropospheric mixing based on man-made ^{14}C, ^{3}H, and ^{90}Sr, *J. Geophys. Res.*, *71*, 2865–2874.
Levin, I., and V. Hesshaimer (2000), Radiocarbon—A unique tracer of global carbon cycle dynamics, *Radiocarbon*, *42*(1), 69–80.
Levin, I., and B. Kromer (2004), The tropospheric $^{14}CO_2$ level in mid-latitudes of the Northern Hemisphere (1959–2003), *Radiocarbon*, *46*(3), 1261–1272.
Levin, I., B. Kromer, H. Schoch-Fischer, M. Bruns, M. Münnich, B. Berdau, J. C. Vogel, and K. O. Münnich (1985), 25 years of tropospheric ^{14}C observations in Central Europe, *Radiocarbon*, *27*(1), 1–19.
Levin, I., J. Schuchard, B. Kromer, and K. O. Münnich (1989), The continental European Suess Effect, *Radiocarbon*, *31*(3), 431–440.
Levin, I., B. Kromer, and R. Francey (1990), Continuous measurements of ^{14}C in atmospheric CO_2 at Cape Grim, in *Baseline Atmospheric Program (Australia) 1988*, edited by S. R. Wilson and G. P. Ayers, pp. 41–42, Bur. of Meteorol., Melbourne, Victoria, Australia.
Levin, I., B. Kromer, and R. Francey (1991), Continuous measurements of ^{14}C in atmospheric CO_2 at Cape Grim, in *Baseline Atmospheric Program (Australia) 1989*, pp. 53–54, Bur. of Meteorol., Melbourne, Victoria, Australia.
Levin, I., R. Bösinger, G. Bonani, R. J. Francey, B. Kromer, K. O. Münnich, M. Suter, N. B. A. Trivett, and W. Wölfli (1992), Radiocarbon in atmospheric carbon dioxide and methane: Global distribution and trends, in *Radiocarbon After Four Decades*, pp. 503–518, Springer, New York.
Levin, I., B. Kromer, M. Schmidt, and H. Sartorius (2003), A novel approach for independent budgeting of fossil fuel CO_2 over Europe by $^{14}CO_2$ observations, *Geophys. Res. Lett.*, *30*(23), 2194, doi:10.1029/2003GL018477.
Levin, I., et al. (2010), Observations and modelling of the global distribution and long-term trend of atmospheric $^{14}CO_2$, *Tellus, Ser. B*, *62*, 26–46.
Liang, Q., A. R. Douglass, B. N. Duncan, R. S. Stolarski, and J. C. Witte (2009), The governing processes and timescales of stratosphere-to-troposphere transport and its contribution to ozone in the Arctic troposphere, *Atmos. Chem. Phys.*, *9*(9), 3011–3025.
Manning, M. R., D. C. Lowe, W. H. Melhuish, R. J. Sparks, G. Wallace, C. A. M. Brenninkmeijer, and R. C. McGill (1990), The use of radiocarbon measurements in atmospheric studies, *Radiocarbon*, *32*(1), 37–58.
Manning, M. R., D. C. Lowe, R. C. Moss, G. E. Bodeker, G. Wallace, and W. Allan (2005), Short-term variations in the oxidizing power of the atmosphere, *Nature*, *436*, 1001–1004.
Marland, G., T. A. Boden, and R. J. Andres (2008), Global, regional, and national fossil fuel CO_2 emissions (1751–2008), in *Trends: A Compendium of Data on Global Change*, Carbon Dioxide Inf. Anal. Cent., Oak Ridge Natl. Lab., U.S. Dep. of Energy, Oak Ridge, Tenn., http://cdiac.ornl.gov/trends/emis/overview_2008.html
Meijer, H. A. J., H. M. Smid, E. Perez and M. G. Keizer (1996), Isotopic characterisation of anthropogenic CO_2 emissions using isotopic and radiocarbon analysis, *Phys. Chem. Earth*, *21*(5–6), 483–487.
Meijer, H. A. J., M. H. Pertuisot, and J. van der Plicht (2006), High accuracy ^{14}C measurements for atmospheric CO_2 samples by AMS, *Radiocarbon*, *48*(3), 355–372.
Münnich, K. O. (1963), Der Kreislauf des Radiokohlenstoffs in der Natur, *Naturwissenschaften*, *50*(6), 211–218.
Naegler, T., P. Ciais, K. Rodgers, and I. Levin (2006), Excess radiocarbon constraints on air-sea gas exchange and the uptake of CO_2 by the oceans, *Geophys. Res. Lett.*, *33*, L11802, doi:10.1029/2005GL025408.
Nydal, R. (1963), Increase in radiocarbon from the most recent series of thermonuclear tests, *Nature*, *200*(4903), 212–214.
Nydal, R. (1968), Further investigation on the transfer of radiocarbon in nature, *J. Geophys. Res.*, *73*(12), 3617–3635.
Nydal, R. (2000), Radiocarbon in the ocean, *Radiocarbon*, *42*(1), 81–98.
Nydal, R., and K. Lövseth (1996), Carbon-14 measurements in atmospheric CO_2 from Northern and Southern Hemisphere sites, 1962–1993, technical report, Carbon Dioxide Inf. Anal. Cent., Oak Ridge Natl. Lab., U.S. Dep. of Energy, Oak Ridge, Tenn.
Pacala, S. W., et al. (2010), *Verifying Greenhouse Gas Emissions: Methods to Support International Climate Agreements*, Natl. Acad. of Sci., Washington, D. C.
Peylin, P., et al. (2011), Importance of fossil fuel emission uncertainties over Europe for CO_2 modeling: Model intercomparison, *Atmos. Chem. Phys.*, *11*, 6607–6622, doi:10.5194/acp-11-6607-2011.
Rafter, T. A., and G. J. Fergusson (1957), "Atom Bomb Effect"—Recent increase of Carbon-14 content of the atmosphere and biosphere, *Science*, *126*(3273), 557–558.
Randerson, J. T., I. G. Enting, E. A. G. Schuur, K. Caldeira, and I. Y. Fung (2002), Seasonal and latitudinal variability of troposphere $\Delta^{14}CO_2$: Post bomb contributions from fossil fuels, oceans, the stratosphere, and the terrestrial biosphere, *Global Biogeochem. Cycles*, *16*(4), 1112, doi:10.1029/2002GB001876.
Rayner, P. J., M. R. Raupach, M. Paget, P. Peylin, and E. Koffi (2010), A new global gridded data set of CO_2 emissions from fossil fuel combustion: Methodology and evaluation, *J. Geophys. Res.*, *115*, D19306, doi:10.1029/2009JD013439.
Rotty, R. M. (1987), Estimates of seasonal variation in fossil fuel CO_2 emissions, *Tellus, Ser. B*, *39*, 184–202.
Sprenger, M., and H. Wernli (2003), A northern hemispheric climatology of cross-tropopause exchange for the ERA15 time period (1979–1993), *J. Geophys. Res.*, *108*(D12), 8521, doi:10.1029/2002JD002636.
Stephens, B. B., et al. (2007), Weak northern and strong tropical land carbon uptake from vertical profiles of atmospheric CO_2, *Science*, *316*(5832), 1732–1735.
Stohl, A., H. Wernli, P. James, M. Bourqui, C. Forster, M. A. Liniger, P. Seibert, and M. Sprenger (2003), A new perspective of stratosphere-troposphere exchange, *Bull. Am. Meteorol. Soc.*, *84*(11), 1565–1573.
Stuiver, M., and H. A. Polach (1977), Discussion: Reporting of ^{14}C data, *Radiocarbon*, *19*(3), 355–363.
Suess, H. E. (1955), Radiocarbon concentration in modern wood, *Science*, *122*, 415–417.
Sweeney, C., E. Gloor, A. R. Jacobson, R. M. Key, G. McKinley, J. L. Sarmiento, and R. Wanninkhof (2007), Constraining global air-sea gas exchange for CO_2 with recent bomb ^{14}C measurements, *Global Biogeochem. Cycles*, *21*, GB2015, doi:10.1029/2006GB002784.
Tans, P. P., A. F. M. de Jong, and W. G. Mook (1979), Natural atmospheric ^{14}C variation and the Suess effect, *Nature*, *280*(5725), 826–828.

Trumbore, S. (2000), Age of soil organic matter and soil respiration: Radiocarbon constraints on belowground C dynamics, *Ecol. Appl.*, *10*(2), 399–411.

Turnbull, J. C., J. B. Miller, S. J. Lehman, P. P. Tans, R. J. Sparks, and J. Southon (2006), Comparison of $^{14}CO_2$, CO, and SF_6 as tracers for recently added CO_2 in the atmosphere and implications for biological CO_2 exchange, *Geophys. Res. Lett.*, *33*, L01817, doi:10.1029/2005GL024213.

Turnbull, J. C., S. J. Lehman, J. B. Miller, R. J. Sparks, J. Southon, and P. P. Tans (2007), A new high precision $^{14}CO_2$ time series for North American continental air, *J. Geophys. Res.*, *112*, D11310, doi:10.1029/2006JD008184.

Turnbull, J., P. Rayner, J. B. Miller, T. Naegler, P. Ciais, and A. Cozic (2009), On the use of $^{14}CO_2$ as a tracer for fossil fuel CO_2: Quantifying uncertainties using an atmospheric transport model, *J. Geophys. Res.*, *114*, D22302, doi:10.1029/2009JD012308.

van der Laan, S., U. Karstens, R. E. M. Neubert, I. T. van der Laan-Luijkx, and H. A. J. Meijer (2010), Observation-based estimates of fossil fuel-derived CO_2 emissions in the Netherlands using $\Delta^{14}C$, CO and ^{222}Radon, *Tellus, Ser. B*, *62*(5), 389–402, doi:10.1111/j.1600-0889.2010.00493.x.

H. D. Graven and R. F. Keeling, Scripps Institution of Oceanography, University of California, San Diego, 9500 Gilman Dr., La Jolla, CA 92093-0244, USA. (hgraven@ucsd.edu; rkeeling@ucsd.edu)

T. P. Guilderson, Center for Accelerator Mass Spectrometry, Lawrence Livermore National Laboratory L-397, 7000 East Ave., Livermore, CA 94550, USA. (tguilderson@llnl.gov)